

# Formation of disks with long-lived spiral arms from violent gravitational dynamics

Francesco Sylos Labini,<sup>1,2,3</sup> Luis Diego Pinto,<sup>4,5</sup> and Roberto Capuzzo-Dolcetta<sup>5</sup>

<sup>1</sup>*Centro Ricerche Enrico Fermi, Via Panisperna 89a, I-00184, Rome, Italia*

<sup>2</sup>*Istituto dei Sistemi Complessi, Consiglio Nazionale delle Ricerche, Via dei Taurini 19, I-00185 Roma, Italia*

<sup>3</sup>*INFN Unit Rome 1, Dipartimento di Fisica, Università di Roma Sapienza, Piazzale Aldo Moro 2, I-00185 Rome, Italia*

<sup>4</sup>*INAF-IAPS, Istituto di Astrofisica e Planetologia Spaziali,  
via del Fosso del Cavaliere, 100, I-00133, Rome, Italia*

<sup>5</sup>*Dipartimento di Fisica, Sapienza, Università di Roma, piazzale Aldo Moro 2, I-00185, Rome, Italia*

(Dated: August 31, 2020)

By means of simple dynamical experiments we study the combined effect of gravitational and gas dynamics in the evolution of an initially out-of-equilibrium, uniform and rotating massive overdensity thought of as in isolation. The rapid variation of the system mean-field potential makes the point like particles (PPs), which interact only via Newtonian gravity, form a quasistationary thick disk dominated by rotational motions surrounded by far out-of-equilibrium spiral arms. On the other side, the gas component is subjected to compression shocks and radiative cooling so as to develop a much flatter disk, where rotational motions are coherent and the velocity dispersion is smaller than that of PPs. Around such gaseous disk long-lived, but nonstationary, spiral arms form: these are made of gaseous particles that move coherently because have acquired a specific phase-space correlation during the gravitational collapse phase. Such a phase-space correlation represents a signature of the violent origin of the arms and implies both the motion of matter and the transfer of energy. On larger scales, where the radial velocity component is significantly larger than the rotational one, the gas follows the same out-of-equilibrium spiral arms traced by PPs. We finally outline the astrophysical and cosmological implications of our results.

PACS numbers: 05.10-a,05.90.+m,04.40.-b,98.62.-g,98.62.Hr

## I. INTRODUCTION

Self-gravitating systems, like other ones that interact with a pair potential decaying with an exponent smaller than that of the embedding space, i.e., with long-range interactions, give rise to macroscopic behaviors that are very different from the ones arising in short-range interacting systems (SRISs). Their origin and properties represent an open theoretical problem because the long-range nature of the interaction displays several behaviors that prevent the use of equilibrium statistical mechanics [1–12]. In particular, the relaxation mechanism driving a long-range interacting system (LRIS) towards a quasiequilibrium state is different from that acting in SRISs. These latter systems typically tend towards thermal equilibrium through a rather rapid collisional relaxation process, in which particles exchange energy predominantly by binary encounters. In this case, to obtain an out-of-equilibrium state it is necessary to force the system with an external field. Instead, LRISs typically show a mean-field (or violent) relaxation process in which their global characteristic quantities (e.g., size, potential gravitational energy, etc.) rapidly vary until they reach a configuration close to a quasistationary state (QSS) [1, 3, 4, 6, 13, 14]. This does not correspond to a true (i.e., thermodynamical) equilibrium state, but it is such that the system is close to be virialized and it is almost time-independent. The violent relaxation phase is then followed by a slow adiabatic evolution driven by collisional processes (see, e.g., Ref. [1, 15]). However, this is not the only way LRISs relax; for instance, in the

cosmological context, self-gravitating systems often relax through a soft and slow relaxation mechanism. This occurs when density fluctuations are long-range correlated so that quasistationary nonlinear structures of increasing size are formed via a bottom-up hierarchical aggregation process [16].

Gravitational relaxation and the formation of QSSs were studied also in (simpler) one-dimensional (1D) systems because in that case one can work out exact solutions [17–21]. For the full three-dimensional problem, given the theoretical difficulties to treat out-of-equilibrium LRIS dynamics, an important tool to study their behaviors is represented by numerical experiments.

While the bottom-up gravitational clustering is usually studied in the context of cosmological simulations, many systematic studies of finite and isolated self-gravitating systems that undergo a global collapse phase have been reported in the literature [22–38]. These experiments use molecular dynamics and start from simple classes of initial conditions (ICs) that do not have the complexity of real astrophysical objects and that, of course, do not aim to represent specific realistic systems. The motivation for their study is to try to improve the understanding of the basic physical mechanisms at play in the evolution of these systems, such as the details of the relaxation toward virial equilibria, the dependence of the equilibria properties on the ICs, phenomena such as symmetry breaking, radial orbits instability, etc. Although, from the statistical mechanics point of view, a complete understanding is still lacking, these studies have shown that the relaxation dynamics acting during a monolithic collapse is very generically the same for a broad class of ICs

and gives rise to quasivirialized configurations with ellipsoidal shapes. However, the QSS properties such as the density and velocity profiles depend on the details of the ICs.

It was recently found that a key role in modifying the simple picture outlined above, is played by the system's initial spatial anisotropy. Indeed, the gravitational collapse phase of initially out-of-equilibrium over-densities amplifies any initial spatial anisotropy both when they are initially at rest or when have a small isotropic velocity dispersion [37, 38]. Initially spherical systems give rise to almost spherical virialized states with a characteristic density profile that decays as  $r^{-4}$  [23, 31, 32]. Systems that initially break spherical symmetry form a two-component state whose inner part is virialized and close to spherical, and its outermost regions are out-of-equilibrium and flat. This occurs because the initial deviation from spherical symmetry is amplified by the collapse mechanism: in particular, the system is stretched along the plane identified by the major and medium axes of the initial configuration<sup>1</sup>.

Moreover, when the initial over-density has a nonzero angular momentum, the gravitational (and dissipationless) collapse gives rise to a thick quasiequilibrium disk surrounded by out-of-equilibrium spiral arms with or without bars and/or rings [39, 40]. These transient structures involve only a fraction of the system's mass and thus represent nonequilibrium perturbations of a substantially virialized state. Such transients, still bound to the system but dominated by radial motions, may continue to evolve for times that are very long compared with the intrinsic gravitational collapse characteristic time  $\tau \sim 1/\sqrt{G\rho}$  — with  $\rho$  being the system's average mass density.

This fast and violent dynamics is rather different from the slow and soft dynamical mechanisms usually considered in astrophysical contexts. Concerning the latter ones, attention was focused on two complementary physical systems. On the one hand, it is well known since the pioneering work in Refs. [41, 42] that galactic disks are remarkably responsive to small disturbances. For this reason there has been a great effort to study the evolution of small-scale disturbances in simplified models of rotating self-gravitating disks with and without a dissipational gas component (see, e.g., Refs. [43–45] and references therein; and Refs. [46, 47] for reviews). These models assume that a disk is already formed and has reached a rotational equilibrium (often in the gravitational field of a spherical halo): the problem that is considered concerns how instabilities can give rise to spiral arms and/or bars. As such instabilities represent small perturbations to the system's gravitational mean field, their effects on

the global system's conditions are small and the overall dynamical mechanism is thus soft.

On the other hand, the question of the disk formation is studied in the cosmological framework. Favored cosmological models, like cold dark matter (CDM) type scenarios, assume matter density fluctuations that are long-range correlated. Such correlations induce a bottom-up hierarchical clustering: that is, a structure of size  $R$  is formed by the aggregation of smaller substructures of size  $< R$  rather than by the global collapse of an over-density of size  $R$ . This kind of hierarchical aggregation, being statistically isotropic, gives rise to quasispherical structures with a quasi-isotropic velocity dispersion. These are the so-called halo structures [48], whose formation is ubiquitous in the context of CDM-type cosmological simulations. The halos are not isolated but evolve in a complex gravitational field generated by neighboring structures and thus are subjected to tidal effects and merging. However, both mechanisms do not violently change the halos mean field potential and thus halos form through a slow and soft dynamical mechanism that does not involve a large variation of their mean field. In this scenario it remains open the question of a disk formation. As first envisaged in Ref. [49], in the cosmological context, a disk can be formed by the dissipational gas collapse: indeed, gas can shock and dissipate energy through radiative cooling, and thus during the gravitational contraction forms a thin disk if it initially has some angular momentum. Such a disk is thus embedded in the much larger gravitational field of the spherical halo structure that is formed by a hierarchical aggregation dynamics: during such a process the system mean field potential does not substantially vary. This situation has motivated the study of simplified ICs (see, e.g., Refs. [50–52]) in which structures are formed via a hierarchical bottom-up aggregation process driven by gravitational clustering with the inclusion of gas that can cool radiatively.

In this work we present several numerical experiments of relatively simple ICs to study the combined effects of gravitational and gas dynamics during the fast and violent phase occurring in the monolithic collapse of an isolated overdensity with some initial angular momentum. Such a process has been overlooked in the literature but, we argue, can give some interesting insights for the formation of real astrophysical structures. Indeed, despite the fact that the problem of the joint effect of gravity and gas dynamics has been studied through numerical experiments of increasing sophistication, the focus has been pointed towards a different kind of physical case, i.e. when a slow and soft dynamical process takes place.

The paper is organized as follows: we start in Sect.II by describing the way in which gravitational and gas dynamics are implemented in the hydrodynamical code we use to make numerical simulations and by presenting the properties of the ICs we have considered. Then in Sect.III we briefly review the main features of the collapse dynamics of an isolated overdensity made of purely self-gravitating particles and show how the results change

---

<sup>1</sup> The simple numerical experiments considered in Refs. [37–40] focused mainly only ellipsoidal ICs, but in a few cases more irregular situations have been considered.

when a gaseous component is added into the system. Finally we draw our main conclusions in Sect.IV.

## II. MODELS AND METHODS

In this section we summarize the main features of the numerical simulations that we have performed with the aim of investigating the collapse and the subsequent relaxation to a quasistationary state of a two-phase (i.e., purely self-gravitating particles and gas) system. In particular the ICs chosen corresponds to an isolated *overdensity* with a simple shape that, in an astrophysical context, can be thought to represent a proto-galaxy detached from the Hubble flow.

### A. Gravitational dynamics of a two-phase system

Our numerical experiments consider isolated systems consisting of  $N$  point like or *gaseous* particles interacting by both body force and surface force (i.e., pressure gradients and viscosity). This particle discretization represents a sampled Lagrangian representation: in particular, we use the smoothed particles hydrodynamics (SPH) approach for the gas dynamics, as described in what follows.

The representative point particles (PPs) and gas particles (GPs) are initially randomly distributed according to a uniform space distribution in the volume corresponding to the initial system. The inner density fluctuations are small enough that an actual *monolithic* gravitational collapse starts from the initial subvirialized state (see below for more details).

All our simulations have been performed by means of the hydrodynamical SPH code **Gadget-3**. This represents an up-to-date version of the already publicly available (and widely used) code **Gadget-2** [53] that has been kindly made available to us by the author. **Gadget-3** computes the hydrodynamical evolution of a gas distribution via a SPH scheme, by subdividing the fluid into a set of interpolating particles whose spatial distribution is proportional to the density field. The GPs interact via Newtonian force and pressure gradient and by the Newtonian force only with the other ensemble of PPs (i.e., point-mass and pressure less objects). The gravitational interaction is evaluated by direct summation over close neighbors and via a multi-polar expansion on a larger scale. In this way, the number of computations is sensibly lower compared to the usual  $N^2$  scaling, characteristic of the direct-summation  $N$ -body algorithms.

The gravitational interaction on the small distance scale is regularized with the so-called “gravitational softening”  $\varepsilon$ : the force has its purely Newtonian value at separations greater than  $\varepsilon$  ( $r \geq \varepsilon$ ) while it is smoothed at shorter separations. The assumed functional form of the regularized potential, is a cubic spline interpolating between the exact Newtonian potential at  $r = \varepsilon$  and a

constant value at  $r = 0$  where the mutual gravitational force vanishes (the exact expression can be found in Ref. [53]).

A detailed study of the parameter space of the code **Gadget-2**, for simulations considering only Newtonian gravity, has been reported elsewhere (see Refs. [36–38, 40]): here we stress that in purely gravitational simulations performed by using only PPs without GPs, we always kept energy, momentum and angular momentum conservation at a level of precision better than 1%. In this work we consider ICs for which the initial virial ratio is

$$\frac{1}{2} \leq Q_0 \equiv \left| \frac{2K(0)}{W(0)} \right| \leq 1 \quad (1)$$

where  $K(t)$  and  $W(t)$  are, respectively, the kinetic and potential energy of the system at time  $t$ . In such cases, the maximum system contraction is of about a factor  $\sim 2$ , i.e., it is not as extreme as for a purely cold collapse (see, e.g., Refs. [24, 31, 32, 35]).

### B. Gas dynamics

The gas component is represented as an inviscid fluid whose time evolution is governed by the set of continuity, Euler (motion) and energy equations. The Lagrangian form of the continuity equation is

$$\frac{D\rho}{Dt} + \rho \nabla \cdot \mathbf{v} = 0 \quad (2)$$

(where  $\rho$  is the fluid density and  $\mathbf{v}$  its velocity) while Euler’s equation of motion is

$$\frac{D\mathbf{v}}{Dt} = -\frac{\nabla P}{\rho} - \nabla \Phi, \quad (3)$$

where  $P$  is the pressure and the body force is given by the gradient of the gravitational potential  $\Phi(\mathbf{r})$ . The above time derivatives are the usual Lagrangian time derivatives along the flow:

$$\frac{D}{Dt} \equiv \frac{\partial}{\partial t} + \mathbf{v} \cdot \nabla. \quad (4)$$

Finally, the thermal energy per unit mass,  $u$ , evolves according to the first law of thermodynamics, *viz.*,

$$\frac{Du}{Dt} = -\frac{P}{\rho} \nabla \cdot \mathbf{v} - \frac{\Lambda(u, \rho)}{\rho}, \quad (5)$$

where  $\Lambda(u, \rho) \geq 0$  represents the radiative *cooling* function per unit volume and we have set the heating function equal to zero. The gas cooling is modeled by adopting the same formalism discussed in Ref. [51], which considers an optically thin medium in ionization equilibrium, characterized by a primordial cosmological composition. Under the, justified, assumption of optically thin medium no heating term is needed in the energy equation. The

cooling rate, expressed as a function of density and temperature, plays an important role since it helps the gas component to lose thermal energy and collapse. Compared to the case in which  $\Lambda(u, \rho)$  is neglected, more compact structures can be then formed. The radiative cooling function  $\Lambda(u, \rho)$  is evaluated by considering several two-body processes involving both helium and hydrogen atoms: collisional excitation, collisional ionization, recombination, and dielectric recombination. Moreover, free-free radiation emission processes are taken into account for all the possible ions.

The cooling rate function,  $\Lambda(u, \rho)$ , used in **Gadget-3** accounts for the various free-bound, bound-bound and free-free processes and is given by the sum of various terms  $\Lambda_i(u, \rho)$  ( $i = 1, 2, \dots, n$ ) each one accounting for the contribution from a specific cooling mechanism. Basically, each  $\Lambda_i(u, \rho)$  term has the form:

$$\Lambda_i(u, \rho) = A_i h(T) n_i n_e \quad (6)$$

where  $A_i$  is a constant,  $h(T)$  is a function of the temperature, while  $n_i$  and  $n_s$  are, respectively, the number density of the particular ‘chemical’ specie involved and the electron number density. The species considered are those typical of primordial gas, i.e., neutral hydrogen and helium ( $\text{H}^0, \text{He}^0$ ) and their ions ( $\text{H}^-, \text{H}^+, \text{He}^+, \text{He}^{++}$ ). Furthermore, a proper treatment of the cooling by molecular hydrogen,  $\text{H}_2$ , is implemented in **Gadget-3** accounting for a nonequilibrium evolution of the abundances of all the ions (see Refs. [54–56]).

As an equation of state we consider the simplest one, i.e.

$$P = (\gamma - 1)\rho u, \quad (7)$$

where  $\gamma$  is the adiabatic exponent. If we take  $\gamma = 5/3$  (mono-atomic ideal gas), the *particle* sound speed is

$$c_s = \sqrt{\frac{5}{3} \frac{P}{\rho}}. \quad (8)$$

As we said above, the **Gadget-3** code calculates the evolution of a gas distribution by using an SPH scheme that was introduced in Refs. [57] and [58] as a Lagrangian method particularly suited to treat the evolution of self-gravitating systems. An SPH representation of a gas is that of an ensemble of moving particles which sample the fluid density distribution. The particles interact with both surface, small-scale, force (pressure and contact forces) and body, large-scale, forces (gravity). In the SPH scheme, each particle is characterized by a specific value of density, pressure gradient, and other relevant hydrodynamical quantities, each evaluated by means of a suitable interpolation over a set of neighbor points. With such a technique the algorithm can work out the quantities useful to solve Eqs.(2)-(7) and to find, for the  $i$ th particle, the density  $\rho_i$ , the velocity  $v_i$ , and the internal specific energy  $u_i$ , which characterize the average status of the system in that specific  $i$ th point. For an exhaustive explanation of the formalism see, e.g., Refs. [59, 60].

Despite we model the gas as an inviscid fluid, the SPH scheme needs an artificial viscosity to treat properly the fluid evolution during strong compression and to avoid nonphysical oscillations. The **Gadget-3** code adopts the same form of artificial viscosity as the **Gadget-2** version, i.e., that suggested in Ref. [61]. Additional details about the artificial viscosity used in our simulations are found in Ref. [53]. Similarly, **Gadget-3** includes the same numerical scheme indicated in Ref. [53] for the implementation of the radiative cooling in SPH, although that was not included in the public release of **Gadget-2**.

### C. Initial conditions

The initial overdensity is characterized by its total mass  $M$ , gravitational radius

$$r_g = \frac{GM^2}{|W(0)|} \quad (9)$$

and total angular momentum  $\mathbf{J}$ . This last is given in the form of a solid body rotation and can be quantified by the nondimensional *spin* parameter [62, 63]

$$\lambda = \frac{|\mathbf{J}|}{G\sqrt{M^5/|W|}}. \quad (10)$$

We have also examined cases where we gave to the system both random motion and solid-body rotation (see discussion in Sect.III I). In this case the initial kinetic energy has a rotational  $K_{rot}$  and a random  $K_{ran}$  term such that

$$\eta = \frac{K_{ran}}{K_{rot}}. \quad (11)$$

We considered prolate, oblate, and triaxial ellipsoids, but hereafter we focus in more detail on the case of a prolate ellipsoid with the three semiaxes such that  $b = c$  and  $a/c = a/b = 3/2$ .

Let  $N_{GP}$  the number of GPs of mass fixed to  $m_{GP}$ . The gas thermal energy per unit mass is

$$u = \chi T, \quad (12)$$

where  $T$  is the absolute temperature and

$$\chi \equiv \frac{k_B}{\mu m_H (\gamma - 1)}, \quad (13)$$

where  $k_B$  is Boltzmann’s constant,  $\mu = 2.33$  is the mean molecular weight [64, 65], and  $\gamma = 5/3$ . We fix  $N_{PP} = N_{GP}$  in the range  $\in [10^5, 10^6]$  and we have taken

$$\psi \equiv \frac{m_{PP}}{m_{GP}} \quad (14)$$

to be  $\psi \approx 10$  that the mass of the gaseous component is  $\sim 1/10$  of the total mass.

For the simulation discussed in more details in what follows, and that we consider as a paradigmatic example

of the class of systems we explored, PPs and GPs are assumed to have the same initial velocity profile, corresponding to a rigid body rotation, and  $T_0 = 40,000\text{K}$  is the initial uniform temperature. The total mass is  $M_0 = 5 \times 10^{10} M_\odot$ , the initial gravitational radius is  $R_g \approx 10$  kpc and the spin parameter is  $\lambda = 0.3$ , corresponding to a virial ratio  $Q \approx 3/4$ .

In summary the parameters that define a simulation in this class of models are 12:  $[M, r_g, Q, \lambda, \eta, a, b, c, T, \psi, \gamma]$ . In order to explore the phase space of this class of systems we note the following:

1. By changing the two parameters that determine the timescale of the collapse  $\tau$  see Eq.(15) below, i.e.,  $M, r_g$ , the typical velocities  $v \sim \sqrt{GM/r_g}$  of the post-collapse system also vary. These parameters can be changed if one wants to simulate a specific astrophysical object: in this work we have considered the case of a medium-size galaxy with  $r_g \sim 10$  kpc and  $v \sim 100$  km/s.
2. The three parameters  $Q, \lambda, \eta$  define the amount of kinetic energy, the angular momentum, and the ratio between rotational and random motions, respectively. We have done several tests to check their effect by taking all other parameters constant.
3. The three parameters  $a, b, c$  determine the shape of the initial ellipsoid. Depending on the initial shape of the overdensity the type of structures that are formed after the collapse may change. We stress that the qualitative features of the collapse dynamics do not depend on these parameters, and thus the results we discuss are quite general for this class of models. However, the quantitative characteristics of the post-collapse systems finely depend on the properties of the ICs and, in particular, on their shape.
4. The three parameters  $T, \psi, \gamma$  define the physical properties of the gas component. If  $T$  is high enough then the thermal energy prevents the collapse while if  $T$  is very low GPs behave initially as PPs. We have also varied  $\psi$  in the range 10 – 50 and we have not observed relevant differences with the case  $\psi = 0.1$ . We have fixed  $\gamma$  so that the gas is a mono-atomic one.
5. Note that we have performed a series of tests by both varying the parameters of the code (i.e., the softening length, the time step accuracy, etc.) and the physical parameters discussed above. We found that the results are stable for variation of these parameters in a broad range and we refer to Refs. [35–38] for a more extensive discussion of the problem of resolution for the crucial case of purely self-gravitating simulations.

### III. DYNAMICS OF THE COLLAPSE AND POST-COLLAPSE STATE

#### A. Formation of disks and structures in purely self-gravitating systems

The violent gravitational dynamics of systems composed by point masses that start from far-out-of-equilibrium configurations generally gives rise to a rich phenomenology, which we summarize below (see for more details Refs. [39, 40]). The ICs consist of a subvirial self-gravitating and isolated system with initial uniform mass density, a nonspherical shape (e.g., an ellipsoid) and some angular momentum assigned in the form of a solid-body rotational velocity field. The overdensity undergoes a monolithic collapse, driven by its own gravitational mean field contrasted by the internal pressure and PP velocity dispersion. This occurs whenever the initial internal density fluctuations are small. Indeed, internal density fluctuations grow during the system's collapse, forming larger and larger substructures. A simple analytic treatment of the growth of fluctuations, neglecting the system's finite size, is based on the linear perturbation analysis of the self-gravitating fluid equations in a contracting background [31]. This is the same approach used in cosmology but for the case of an expanding universe [16] (a more detailed approach that considers the system's finite size may be found in Ref. [24]). In these conditions the growth of perturbations is controlled by the amplitude of the initial fluctuations and by their correlation function.

The collapse characteristic time-scale for a system with uniform density is of the order of

$$\tau \sim \frac{r_g^{3/2}}{\sqrt{GM}}, \quad (15)$$

where  $r_g$  is the initial gravitational radius of the system and  $M$  is its mass. The criterion to define the time  $t^*$  when the collapse is halted is the following [31, 66]:  $t^*$  corresponds to the time when the size of nonlinear perturbations (defined, e.g., as the scale  $\lambda_0$  at which the normalized mass variance is equal to one) becomes of the order of the system's gravitational radius  $r_g$ . Thus, if the initial fluctuations have a small enough amplitude and/or they are not strongly correlated, then  $t^* \approx \tau$  so that the system has had time to contract by a large factor. Otherwise, if density fluctuations have a large amplitude and/or are spatially correlated, bottom-up perturbations grow rapidly enough that a large contraction does not occur because of the quicker system fragmentation into many substructures. In that case clustering proceeds through a bottom-up aggregation process, i.e., a *slow and soft* dynamics. If the system is initially not spherically symmetric, the monolithic collapse eventually leads to the formation of a quasistationary thick disk, in which rotational motions dominate but with a large velocity dispersion. In the outermost regions spiral arms

are formed, possibly with bars and/or rings, in which particles do not follow steady circular orbits because their velocity has both a rotational and a radial component. While, globally, the system reaches a quasiequilibrium state close to a virial configuration, its external parts, which contain only a fraction of the system mass, expand (i.e., they are out-of-equilibrium) for a much longer time than the gravitational collapse timescale  $\tau$ . Let us further consider the origin of the out-of-equilibrium structures.

The variation of the mean gravitational field during the collapse triggers a change of the particle energy distribution, which in turn, induces a reassessment of the system's phase-space macroscopic properties. This mechanism is both rapid and energetically violent, and it works as follows. Although initially all particles are bound, during the collapse a fraction of them can gain some kinetic energy. The mechanism of particle energy gain originates from the coupling of the growth of inner density fluctuations with the finite size of the system. Particles originally placed close to the system boundaries develop a net lag with respect to the bulk because the density in the outer regions of the system decreases during the collapse as a consequence of the growth of density fluctuations and of the corresponding peculiar motions. While in an inner shell at  $R$  the flow of particles from  $< R$  or  $> R$  is statistically symmetrical, in the outermost regions there is an asymmetry because of the system's finite size: for this reason, during the collapse, there is a net outflow of particles in the outer regions so that their density becomes smaller than that in the inner ones. Correspondingly the collapse time becomes larger than that of the others, and thus a time lag is developed. Thus such particles arrive at the system center when the others are already re-expanding. In such a way, these particles move for a short time interval in a rapidly varying gravitational field and for this reason they can gain kinetic energy. In consequence of this mechanism the whole particle energy distribution largely changes. Given the complex interplay between the growth of density fluctuations and the system's finite size, both the IC shape and the nature of correlations between density fluctuations determine the details of this process. The larger the deviation from spherical symmetry of the ICs, the larger the spread of particles' arrival times at the center and thus the larger the particles' energy gain [37].

The initial anisotropic distribution is thus amplified by the collapse mechanism because the particles that initially lie in the outermost regions, and that are thus strongly anisotropically distributed if the system breaks spherical symmetry, get the largest energy increase. For instance, in the case of a simple prolate ellipsoid with semiaxis  $a > b = c$  these particles are initially located in the region  $a < r < b = c$  [37], and they are not spherically symmetric either after the collapse. Indeed, the collapse amplifies their initial asymmetry, because of such positive energy gain, so that the final distribution becomes very anisotropic, with a shape close to a thick disk whose minor axis coincides with the rotation axis as

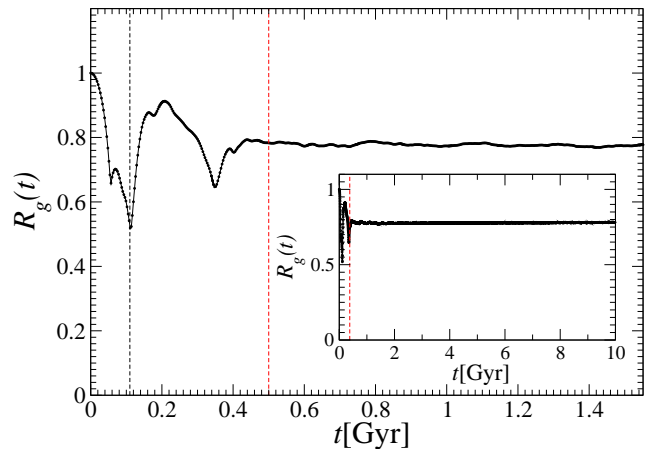


FIG. 1. Time evolution of the normalized gravitational radius  $R_g(t)$  (see Eq.(16)). Results for longer times are illustrated by the inner panel. The vertical lines correspond to  $t = \tau$  and  $t = 5\tau$ .

the system is stretched along the plane identified by the major and medium axes of the initial configuration. In addition, such a disk is surrounded by out-of-equilibrium spiral arms that are formed because the most energetic particles, having both a transverse and a radial velocity component, move in an almost central gravitational field and thus conserve angular momentum [39].

In summary, the asymmetric collapse and re-expansion induce a mass loss from the system, as some particles may gain enough kinetic energy to escape from it, and this leads to a new, marginally stable, configuration of lower energy. If the initial angular momentum is nonzero, such a state forms a thick disk whose minor axis is oriented parallel to the angular momentum.

## B. Evolution of global system quantities

For the initial conditions described in Sect.II C the collapse and the subsequent relaxation to a QSS, in the system internal region, is characterized by three different time phases. They can be identified (see Fig.1) by analyzing the behavior of the system's dimensionless gravitational radius [18]:

$$R_g(t) = \frac{W(0)}{W(t)}, \quad (16)$$

where  $W(t)$  is the gravitational potential energy at time  $t$  and  $W(0)$  that at the initial time. The first phase corresponds to an initial decrease of  $R_g(t)$  up to when it reaches its absolute minimum at  $t \approx \tau \approx 0.1$  Gyr where  $\tau$  is given by Eq.(15). This phase is thus driven by an overall contraction of the system and, as we will discuss below, by the dissipation of the gas internal energy. The gravitationally collapsing nongaseous matter rapidly changes its shape becoming flat — along the rotation axis — to a lesser extent compared to the gas distribution.

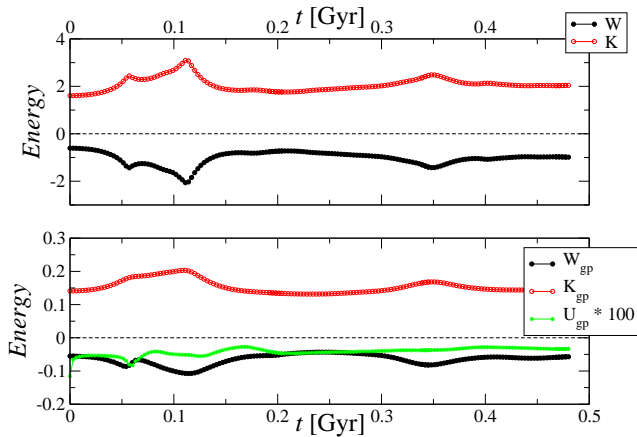


FIG. 2. Upper panel: time evolution up to  $t = 5\tau \approx 0.5$  Gyr of the kinetic ( $K$ ) and potential energy ( $W$ ), for all particles. Note that both energies are normalized to the initial potential energy, Bottom panel: time evolution of the kinetic ( $K_{gp}$ ), potential ( $W_{gp}$ ), and thermal energy ( $U_{gp}$  — multiplied by  $10^2$ ) for the GPs.

Together with the gravitational radius, the mean gravitational potential energy of the system decreases. Such a rapid potential variation triggers a large change of the particles' total energy<sup>2</sup> distribution and thus, in turn, of the system's phase-space properties.

This first phase is then followed by a second one, for  $\tau < t < 5\tau \approx 0.5$  Gyr, characterized by a few damped oscillations of  $R_g(t)$  and of the total gravitational potential energy. During such oscillations the system shows rapidly varying transient configurations both in real and in velocity space. Then, in the third phase, for  $t > 5\tau$ , the system is relaxed to a QSS in its inner region and  $R_g(t)$  has reached its asymptotic value. However, in the outermost regions there are out-of-equilibrium structures that yet continue to evolve for times  $t \gg \tau$ .

Figure 2 shows the temporal evolution of the system's kinetic, potential energy (top panel) and of the solely gas component (bottom panel) together with its thermal energy. The kinetic  $K$  and potential energy  $W$  of the PPs are initially of the same order of magnitude as the virial ratio is  $Q \approx 3/4$ . Even for the GPs the kinetic energy  $K_{gp}$  is of the same order of the potential energy  $W_{gp}$  amounting to  $\sim 10\%$  that of the PPs. In addition, the total thermal energy  $U_{gp}$  of the GPs gives a negligible contribution to the GPs kinetic energy, being  $U_{gp}$  about the 1% of  $K_{gp}$ . Indeed, given the values of  $T, M, r_g$  we have used the ratio between the initial internal energy per unit mass and the typical particle's potential energy

<sup>2</sup> The total energy of a particle, per unit mass, is  $\epsilon = (1/2)v_i^2 + \phi_i + u_i$  where  $v_i$  is the velocity of the  $i$ th particle,  $\phi_i$  its gravitational potential per unit mass and  $u_i$  the specific internal energy (that is zero for a PP).

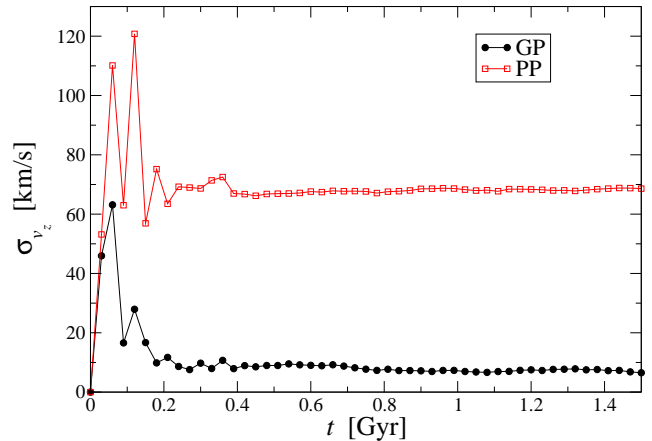


FIG. 3. Time evolution of the vertical velocity dispersion  $\sigma_{v_z}$ . Results for both gas and particle components are shown.

is

$$\frac{u}{|\phi_0|} = \frac{\chi T}{\frac{GM}{r_g}} \approx 10^{-2}. \quad (17)$$

### C. The three dynamical phases

During the first phase the GP develop a very flat distribution along the plane orthogonal to the rotation  $Z$ -axis. This occurs because the gas quickly increases its central density during the rapid system's collapse. When the gas becomes dense enough the radiative cooling function  $\Lambda(u, \rho)$  (see Eq.5), according to the schemes adopted in then literature and used in this work, becomes proportional to  $\rho^2$  and the cooling processes acquire more and more efficiency ( see Sect.II B). Thus, thermal energy may be easily dissipated reducing the  $Z$  component of the velocity as a particle crosses the  $XY$  plane. In such a way the GP component develops a much flatter distribution than that of the PP component. Such further dissipation lets the GPs lower their temperature. For this reason, together with a decrease of the vertical thickness, the GPs drastically reduce their vertical velocity dispersion at  $t \approx \tau$  Gyr (see Fig.3).

The probability density function (PDF) of the temperature  $P(T)$  of the GPs is shown in Fig.4: we can observe a progressive redistribution of the SPH particles temperatures towards lower values. At  $t = 0.3$  Gyr the distribution  $P(T)$  is already peaked at  $\sim 18,000$  K; then, at longer times, the GPs slowly cool down so that the maximum of  $P(T)$  reaches  $T \approx 15,000$  K. In consequence of the overall system's collapse also the PPs rapidly change their spatial distribution by contracting along the  $Z$  axis, although forming a less flat structure compared to the gaseous disk. As the PP component is gravitationally dominant, this contraction modifies the system's mean gravitational potential (see Fig.5).

The differences acquired by the vertical configurations

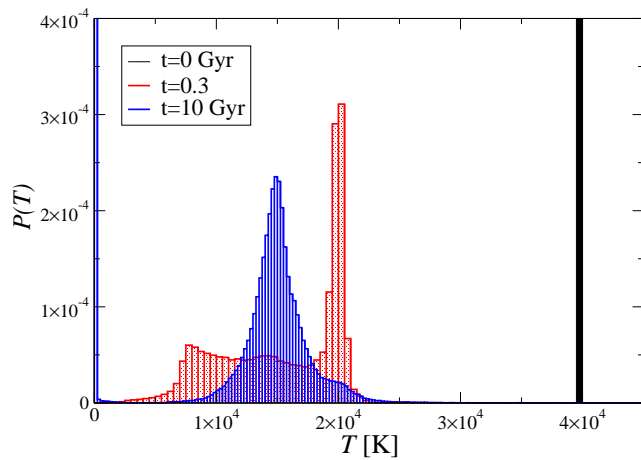


FIG. 4. PDF of the gas temperature at different times:  $t = 0, 0.3, 10$  Gyr. The GP initial temperature distribution is plotted too, and it is a Dirac  $\delta$ -function centered at  $T = 40,000$  K.

of the density distributions of the two components are clear in Fig.6, which shows the vertical density profile of both the PPs and the GPs: they both display an exponential decay

$$n(z) \sim \exp(-z/z_0)$$

with  $z_0 \approx 0.7$  kpc for the PPs and  $z_0 \approx 0.12$  kpc for the GPs. Thus, at  $t \geq 0.2$  Gyr the GPs form an extremely flat disk and the PPs a thicker disk: when the density increases such that the cooling becomes very efficient, the gas component decouples from the PPs component and it starts to have a different time-evolution. Note that PPs and GPs have a different velocity dispersion and this is the reason why the GPs do not follow the same trend of the PPs in their vertical density profile (see Fig.6).

The difference in the motion of GPs and PPs after the collapse can be noticed by looking at the profile of the azimuthal velocity  $v_\phi(R)$ , i.e., the mean azimuthal velocity evaluated in concentric circular coronas in the disk as a function of the two-dimensional (2D) disk radius  $R$ , and of its dispersion profile  $\sigma_{v_\phi}(R)$ <sup>3</sup>. In particular, the amplitude of  $v_\phi(R)$  of the GPs component is larger (by about a factor  $\sim 2$ ) than that of PPs, while the dispersion is smaller by a factor  $\sim 6 - 8$  (see Fig.7). Such a noticeable difference is due to the fact that the motion of the gas component, being confined on a thin disk, is much more coherent than that of nongaseous matter. The signature of such a coherence is shown by the PDF  $P(v_\phi)$  of the azimuthal velocity: this is more peaked for GPs than for PPs (see Fig.8). Note that the maximum

<sup>3</sup> Unless differently specified we adopt a cylindrical coordinates system  $(R, \phi, z)$ .

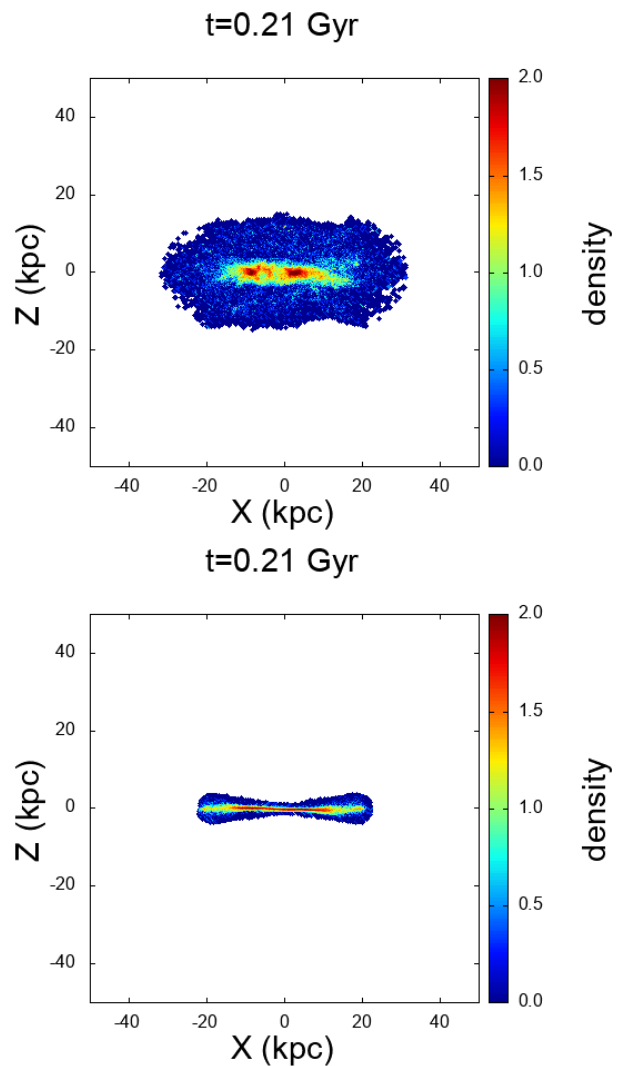


FIG. 5. Density map of the PP component (upper panel) and of the GP component (bottom panel) on the  $XZ$  plane at time  $t = 0.21$  Gyr. The density is computed in cells in the  $XZ$  plane and it is integrated over the  $Y$  axis; the color scale is logarithmic.

radial anisotropy

$$\beta = 1 - \frac{\langle v_t^2 \rangle}{2\langle v_R^2 \rangle} \rightarrow 1, \quad (18)$$

is reached in the outermost regions of the system corresponding to the peak of  $P(v_\phi)$  for  $v_\phi \rightarrow 0$ . Indeed, when a particle increases its distance from the system's center, it decreases its tangential velocity because it approximately moves in a central potential conserving its angular momentum.

The radial velocity profile  $v_R(R)$  (computed in circular coronas) and the relative dispersion profile  $\sigma_{v_R}(R)$  of both the PPs and GPs show a large-distance time-dependent tail (see Fig.9): this is due to the out-of-equilibrium particles that have gained the largest amount

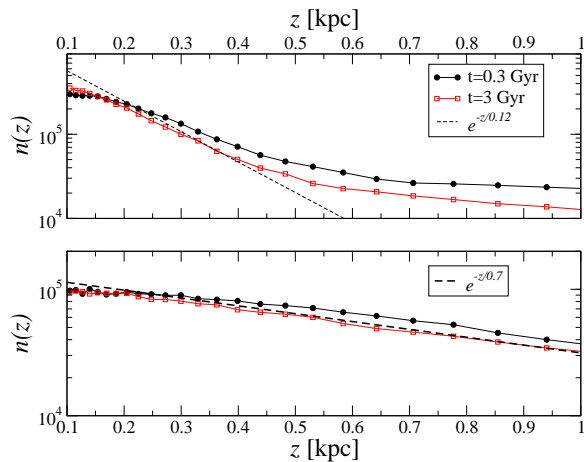


FIG. 6. Time evolution of the vertical number density profile of the GPs (upper panel) and PPs (bottom panel) at  $t = 0.3$  Gyr and  $t = 3$  Gyr. As a reference we report (dashed lines) an exponential decay  $n(z) \sim \exp(-z/z_0)$  where  $z_0 = 0.12$  kpc for the gas component and  $z = 0.7$  kpc for the nongaseous component.

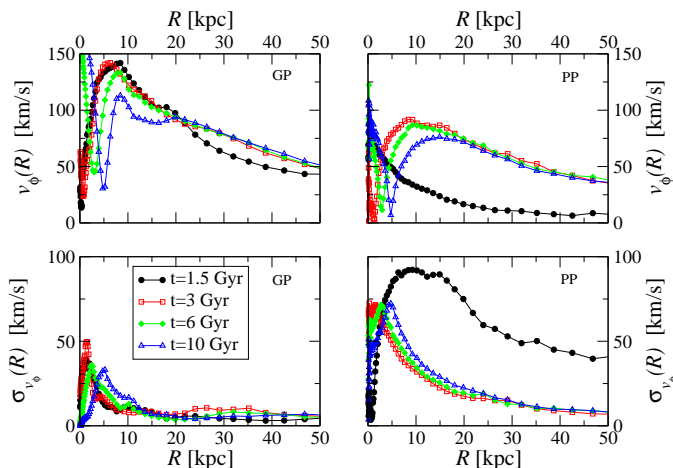


FIG. 7. Azimuthal velocity profile (upper panels) and its dispersion profile (bottom panels) for the GPs (left panels) and PPs (right panels) at different times (see upper left labels).

of energy during the collapse phase. At small distances the dispersion  $\sigma_{v_R}(R)$  is also larger, by a factor 2-3, for PPs than for GPs. The PDF of the radial velocity is shown in Fig.10: one may note that while PP have an approximately symmetric PDF the GPs show an asymmetrical one with a persistent tail both at positive values.

At the end of the second phase, at  $t \approx 5\tau \approx 0.5$  Gyr, the system has almost reached its asymptotic state. In particular, the particle energy PDF  $P(\epsilon)$  quickly relaxes to an almost time-independent shape that determines the properties of the QSS (see Fig.11). This distribution has undergone to a substantial change at  $t \sim \tau$  in consequence of the rapid variation of the system's mean gravitational field. Indeed, particles moving in a rapidly

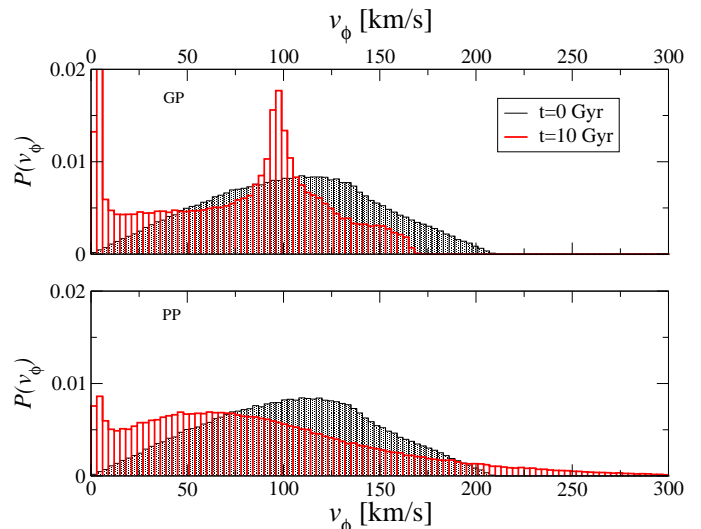


FIG. 8. PDF of the azimuthal velocity for GPs (upper panel) and PPs (bottom panel) at  $t = 0$  and  $t = 10$  Gyr.

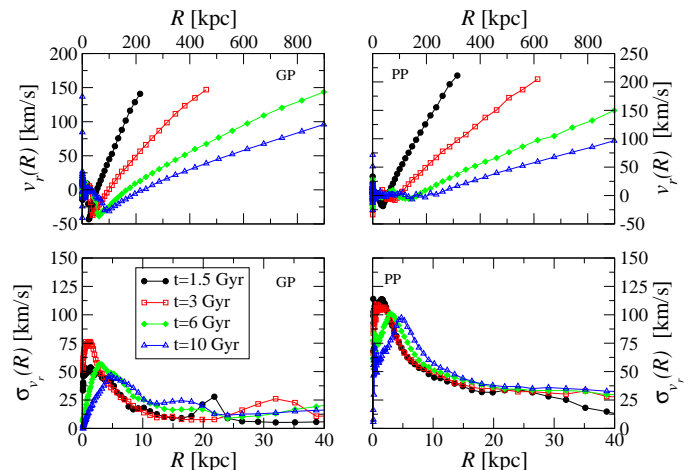


FIG. 9. Radial velocity profile (upper panels) and its dispersion profile (bottom panels) for the GPs (left panels) and PPs (right panels) at different times (see labels).

varying potential field do not conserve energy and the variation of the mean-field potential triggers the change in the system's macroscopic properties as we discussed above for the PP case. The energy change is, however, different for the PPs and the GPs, reflecting their different dynamical evolution. In particular, because GPs can dissipate energy they have an energy distribution with a negative tail that is more extended for than for PP. Note that the fraction of the GPs mass for  $r > 10$  kpc is less than 10% of the total GPs mass. The boundary conditions are open and thus the escaping particles increase their distance indefinitely.

The density profile (see Fig.12) shows a flat core and an approximate  $n(R) \sim R^{-4}$  decay at large distances: both behaviors are typically formed after a violent enough collapse [32]. Note that the large-distance tail continues to

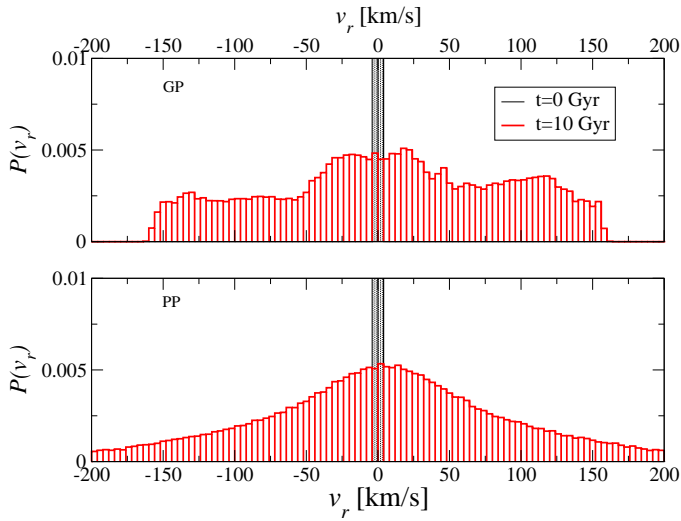


FIG. 10. PDF of the radial velocity for GPs (upper panel) and PPs (bottom panel) at the initial time and  $t = 10$  Gyr.

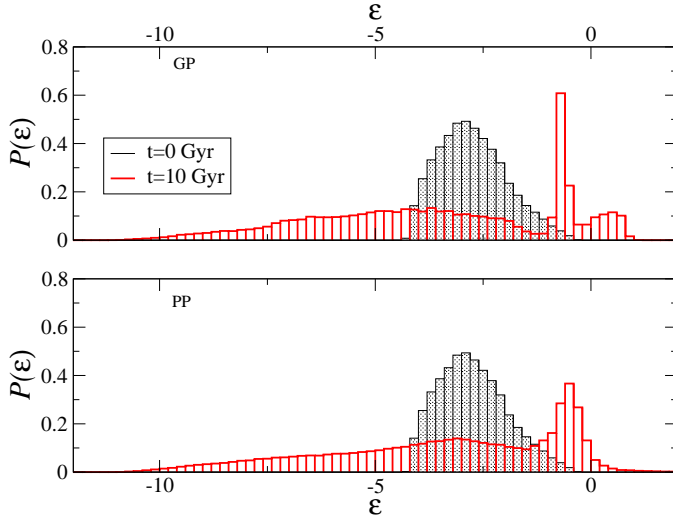


FIG. 11. Energy distribution at  $t = 0$  and  $t = 9$  Gyr for the GPs (upper panel) and PPs (bottom panel).

evolve for long times, due to the particles with energy close to or larger than zero. Finally, the behavior of integrated mass versus radius is reported in Fig.13: we show both the integrated mass  $M(R)$  computed in a tiny cylinder with thickness  $\Delta Z = 2$  kpc (in cylindrical coordinates) and the integrated mass  $M(r)$  computed in spheres. The difference between the two is due to the fact that the PP is not confined on the thin disk as its mass is distributed in a larger volume around it.

#### D. The inhomogeneous gas velocity field

Given the complex dynamical mechanism at work, the velocity field of the system formed after the collapse is

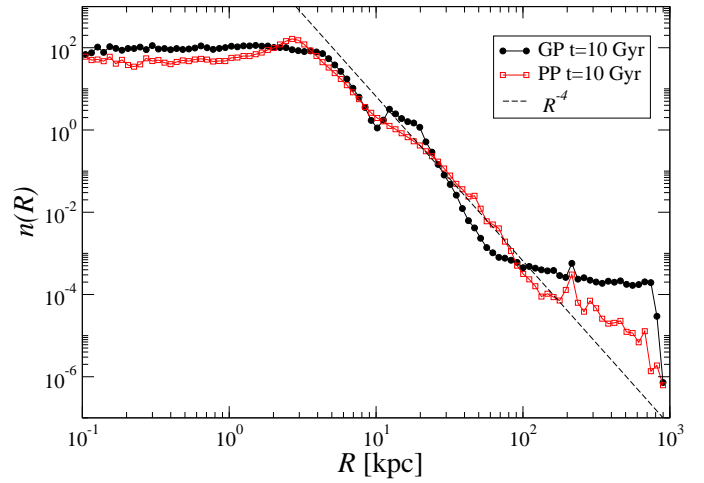


FIG. 12. Number density profile for both the PPs and GPs

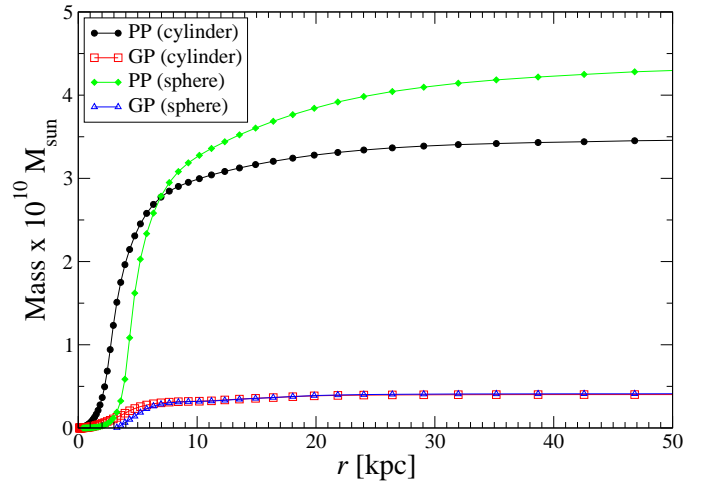


FIG. 13. Integrated mass as function of the radius of a cylinder of thickness  $\Delta Z = 2$  kpc and in spheres. Note that the mass is in units of  $10^{10} M_{\odot}$ .

rather heterogeneous: not only the PPs and the GPs have a different velocity field but, in both cases, its properties depend on scales. Let us now focus on the GP component given that the PP component shows the evolution we described above for the case of a purely self-gravitating collapse: GPs represent indeed a small perturbation of the system mass and thus the evolution of the PPs is unperturbed by the presence of the GPs.

Figures 14-16 show the projection (on the  $XY$  plane) of several snapshots, with a color code corresponding respectively to the logarithm of the number density integrated over the  $Z$  axis and the radial and the azimuthal velocity component of the gas distribution<sup>4</sup>. One may

<sup>4</sup> Movies of these runs can be found at the URL:

note a rapid initial change of shape and then the relaxation to a QSS, i.e., a phase in which the system inner disk becomes almost stable. In particular, for  $0.1 \text{ Gyr} < t < 0.3 \text{ Gyr}$  the GP forms almost 1D filaments that get later warped forming a sort of spiral arms. Note that the core and the spiral structures do not rotate with synchronized rotation as the tangential velocity is not constant at different distances. Such a disk has major axis  $\sim 14 \text{ kpc}$  and minor axis  $\sim 6 \text{ kpc}$  so that its ellipticity is  $e \approx 0.4$ , i.e., its size is of the same order of magnitude of the initial size of the system. Instead, the ellipticity is related both to the major to minor axis ratio of the initial system and to the amplitude of the initial angular momentum. These parameters control how violent the collapse is and thus how large is the particle energy gain as a function of direction. The smaller the angular momentum, the stronger the collapse and the larger is expected to be the ellipticity of the quasistationary disk formed by the gas.

From the visual inspection of these figures one may note that the compact and elliptical gaseous disk is surrounded by a sparser region in which there are long-lived but changing in time (i.e., nonstationary) spiral arms. There is then, in the outermost regions of the systems (not visible in these figures; see below for a discussion), a fraction of particles that is evolving in an out-of-equilibrium manner. Let us now consider the time evolution of the structures present in these three regions. We have identified particles belonging to the three mentioned regions in a snapshot at  $t = 6 \text{ Gyr}$ , where they can be easily disentangled, and we have traced backward and forward their evolution at the initial time and at  $t = 10 \text{ Gyr}$ .

### E. Energy and velocity probability distributions

Both the velocity and energy PDF are rather different in the three regions. One may note (see Fig.17) that particles in the inner region, i.e., the elliptical disk, have a very spread PDF  $P(v_R)$  with a variance of  $\sigma_{v_R} \sim 50 \text{ km/s}$ . In the intermediate region  $P(v_R)$  is still peaked around zero but with a smaller dispersion of about  $\sigma_{v_R} \sim 10 \text{ km/s}$ . In the outermost regions of the system  $P(v_R)$  develops a long tail toward large  $v_R$  values, which however involves a small fraction (i.e.,  $\sim 10\%$ ) of the gas matter. Complementary to this tail the PDF of  $v_\phi$  develops a peak for  $v_\phi \rightarrow 0$  for the reasons we have already discussed above. The PDF of the azimuthal velocity is peaked at high values of  $v_\phi$  in the intermediate region, while in the inner region particles have smaller azimuthal velocities with a larger dispersion.

By considering the behavior of the energy per unit mass distribution (see Fig.18) in the three different regions we can conclude that: particles in the inner region

(the disk) are strongly bound and have decreased their energy since the initial time and particles in the intermediate region (the arms) have energy close to, but smaller than, zero and have increased their energy from the initial state. Finally particles in the outermost regions are those which have mostly increased their energy, and some of them can even escape from the system. Thus, there is a correlation between the energy gain or loss rate and the distance of the particles from the system center: the origin of such a correlation can be traced back to a particle's initial position.

Indeed, Fig.19 shows the conditional probability for a particle of being member of a given group (i.e., inner disk, arms and outermost regions) as a function of its initial position. The conditional probability that a randomly chosen particle at distance  $r$  in the initial configuration is in the outer region at  $t = 9 \text{ Gyr}$  is much larger if it was initially in the outermost shells. On the other hand if a particle was initially in the inner regions of the system, the probability that it remains there is larger than for particles initially placed in the outer regions. Particles in the arms were initially placed in an intermediate region.

### F. Origin of the spiral arms

The formation of such a correlation implies that the change of energy and velocity during the collapse is correlated with the particle initial position. This implies that groups of particles coming from specific regions of the systems have a similar dynamical history and thus remain correlated during the evolution. Such a correlation is thus the specific signature of the monolithic collapse. The underlying mechanism was outlined above: particles in the outer region of the initial distribution increase their energy because are still collapsing when the others (that will decrease their energy) are already re-expanding.

Figure 20 shows the evolution of spiral arms in the  $XY$  plane. The particles that form the arms are identified in an evolved snapshot, at  $t = 6 \text{ Gyr}$ : the position of these same particles is then tracked back to  $t = 0$  and forward to  $t = 10 \text{ Gyr}$  to reconstruct the temporal evolution of the arms. One may see that particles move in a coherent way and that the majority of the particles in a given arm remain the same from its formation till the end of the simulation: that is the arms are not density waves as they involve the motions of particles. The correlation in both configuration and velocity space is developed during the collapse phase and persists over the whole run. On the very long timescales, i.e.,  $t \gg 10 \text{ Gyr}$ , the arms will be washed out for the effect of the velocity dispersion inside them.

Particles forming the arms were originally in the outer region of the system and thus their energy changes by a positive amount that is smaller than the absolute value of the energy variation of particles in the inner disk (see Fig.18). For this reason their radial velocity remains

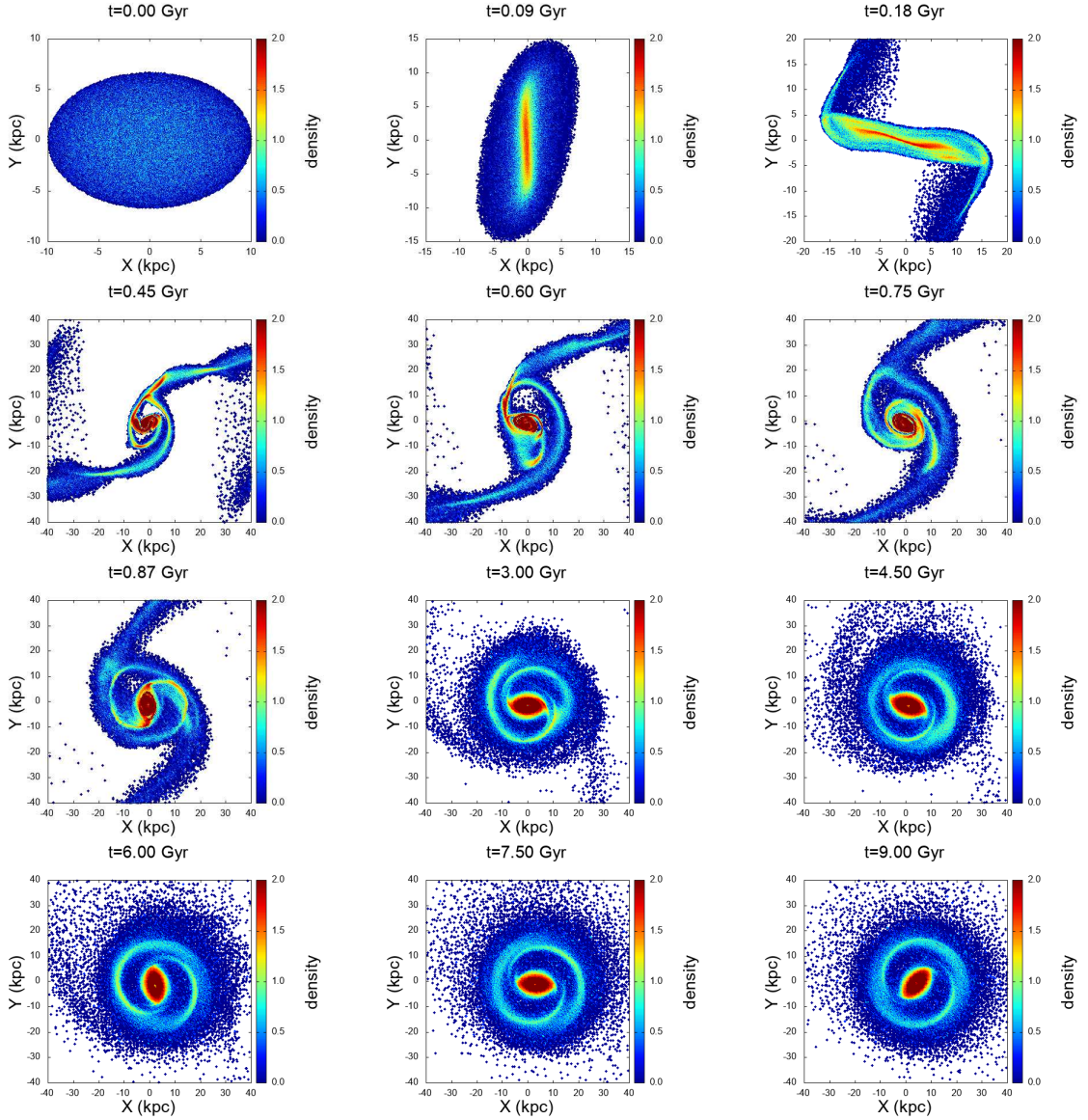


FIG. 14. Projection of various times slices of the GP component on the  $XY$  plane: the color code corresponds to the logarithm of the density integrated over the  $Z$  axis. The corresponding time is reported at the top of each each panel.

peaked at zero, while that of the inner disk particles spreads and the PDF is close to uniform. Given that the azimuthal velocity is larger than the radial velocity, the orbits are closer to circular ones than those of the inner disk particles. The symmetry of the arms is related to the symmetry of the initial conditions, as the two arms are formed by particles initially lying in a symmetric position along the system's major axis. During the evolution, the particles in the arms increase their spread in position and velocity and for this reason the arms are expected to be washed out in the long-run. However, for what concerns the range of times we have considered (i.e.,  $\sim 10$  Gyr) the arms remain well formed.

It is interesting to note that in the 2D phase space of 1D gravitational systems, spiral structures are formed as

a result of filamentary patterns that appear due to differential rotation of an incompressible fluid [17–21]. Such spiral structures are apparently similar to those observed in the present work in the projected 2D plane occupied by the cooled compressed gas; whether the dynamical origin of these spiral arms is the same the two cases is, however, an open question and requires a complete analysis of the 6D phase-space: this goes beyond the scope of this work. In what follows we will discuss only the properties of some projections of the 6D phase-space.

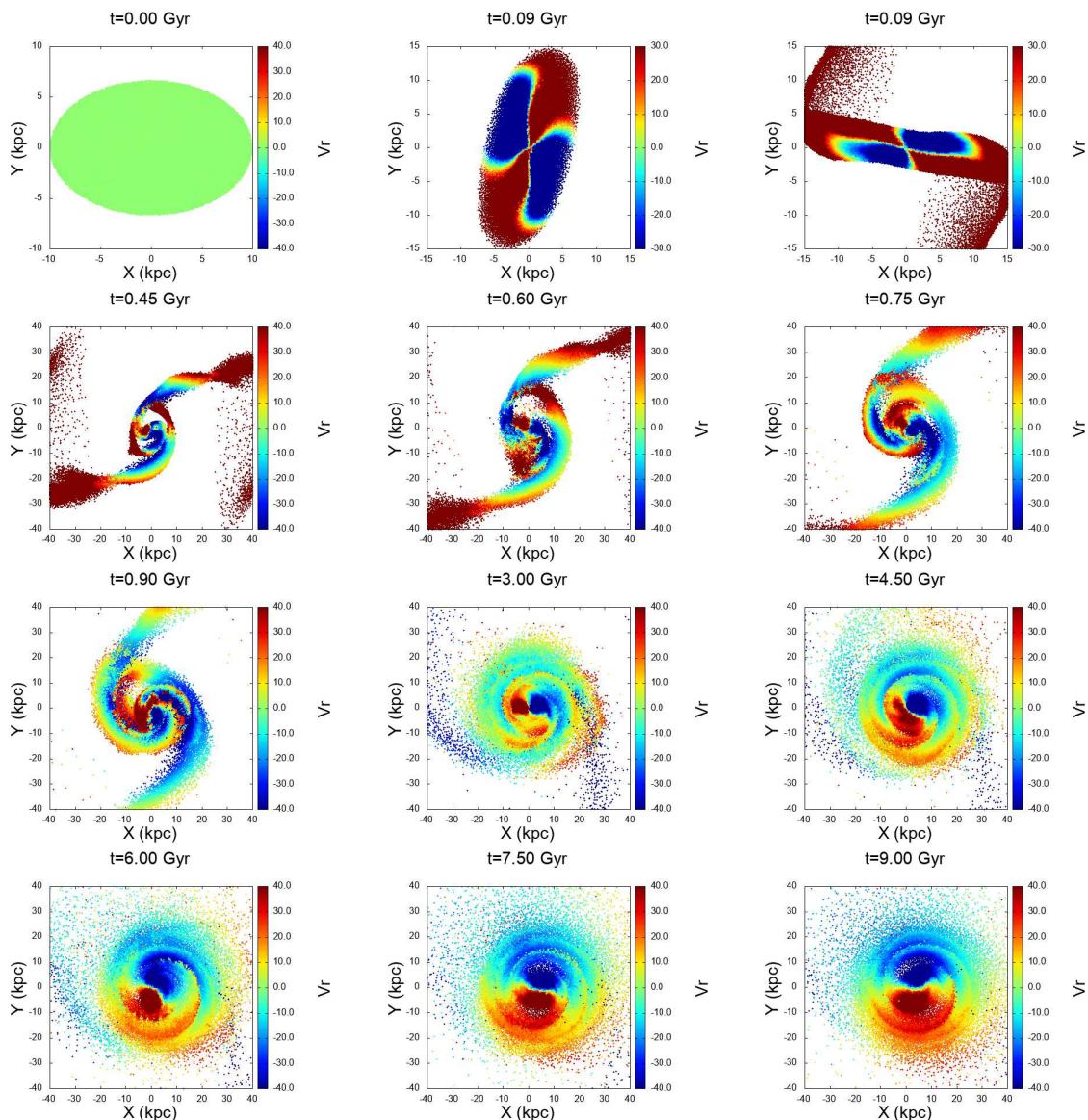


FIG. 15. Projection of various time slices of the GP component on the  $XY$  plane: the color code corresponds to the modulus of the radial velocity. The corresponding time is reported at the top of each panel.

### G. Structures in phase-space

The projection of the phase space into the  $v_R - v_\phi$  plane (see Fig.21) reveals the presence of some nontrivial structures. It also reveals most notably that particles belonging to the inner disk have a spread distribution in both velocity components with some correlated structures which reflect the elliptical motions, and particles in the arms occupying a very localized region in which  $v_\phi$  is close to maximum and  $v_R$  close to zero: such a region is, however, not symmetrical either with respect to  $v_\phi$  or to  $v_R$  and there are several sub-structures in it. Such sub-structures in phase-space correspond to the presence of the real-space structures, i.e., the spiral arms. Finally particles in the outer regions can be recognized by hav-

ing a correlated stream corresponding to a decrease of  $v_\phi$ , when  $v_R$  increases, that is, as a consequence of particles' angular momentum conservation.

Let us now focus on the inner elliptical disk. It is not surprising that particles move on elliptical orbits in this region as shown by Fig. 22: one can see also that there is an overall precession of the whole disk. These motions can be easily explained by considering that when a particle moves in an elliptical orbit from the perigee to the apogee it increases its distance from the center and thus it has a positive radial velocity component. Clearly, the opposite occurs when a particle moves from the perigee to the apogee. It should be stressed that GPs move in the gravitational potential of the whole system that is dominated by the PP distribution that, as mentioned above,

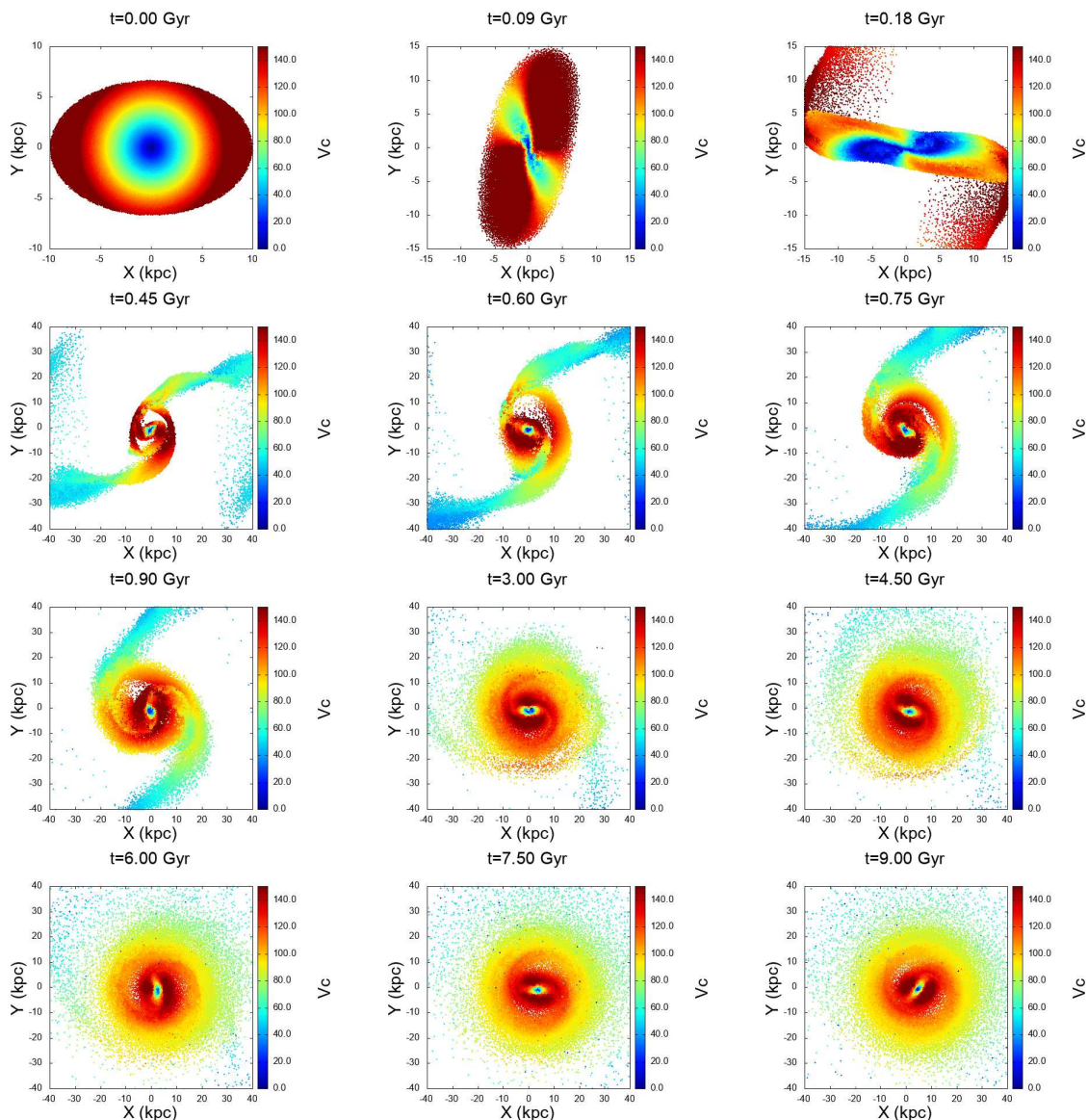


FIG. 16. Projection of various times slices of the GP component on the  $XY$  plane: the color code corresponds to the modulus of the azimuthal velocity. The corresponding time is reported at the top of each panel.

also form a disk (although with a larger thickness). These particles are strongly bound and confined in phase space and their velocity is predominantly oriented along the azimuthal direction, but a relatively large radial component was developed in the second phase of the collapse (i.e.,  $\tau < t < 5\tau$ ). For this reason, after the transient phase, they relax to elliptical orbits.

Finally Fig. 23 shows the comparison of the GP and PP distributions at large distances from the center of mass of the system. The spiral arms in the outermost regions are out-of-equilibrium and dominated by radial motions; GP trace the same structures formed by the heavier PP, although the latter component, having a larger velocity dispersion, traces more spread arms than the former one.

## H. Jeans' equation

The circular velocity is defined to be the velocity with which test particles would move on circular orbits at radius  $R$  from the center of a self-gravitating disk with an axisymmetric gravitational potential  $\Phi$  [46]:

$$v_c^2(R) = \left( R \frac{\partial \Phi}{\partial R} \right)_{z \approx 0}. \quad (19)$$

Let us assume that the system is in a steady state and that is axisymmetric so all derivatives with respect to  $t$  and  $\phi$  vanish. Under these hypotheses and by neglecting collisions, one may derive from the collisionless Boltzmann equation, the Jeans equation which links the density and the moments of the velocity distribution to the

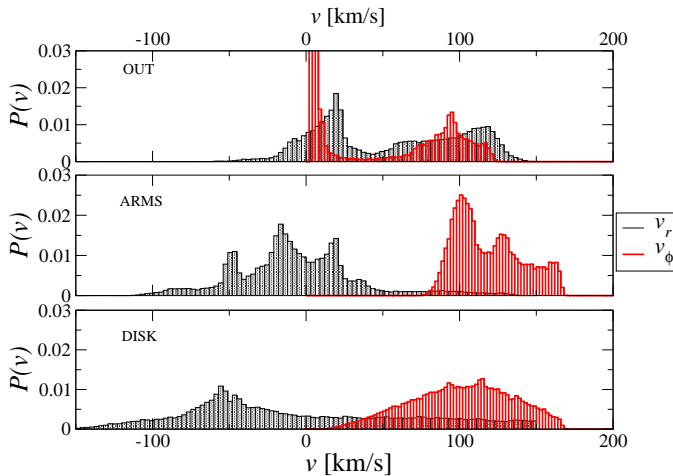


FIG. 17. PDF at  $t = 9$  Gyr of  $v_R$  (black lines) and  $v_\phi$  (red lines) respectively in the inner region (the disk, bottom panel), intermediate region (the arms, middle panel), and outermost region (upper panel)

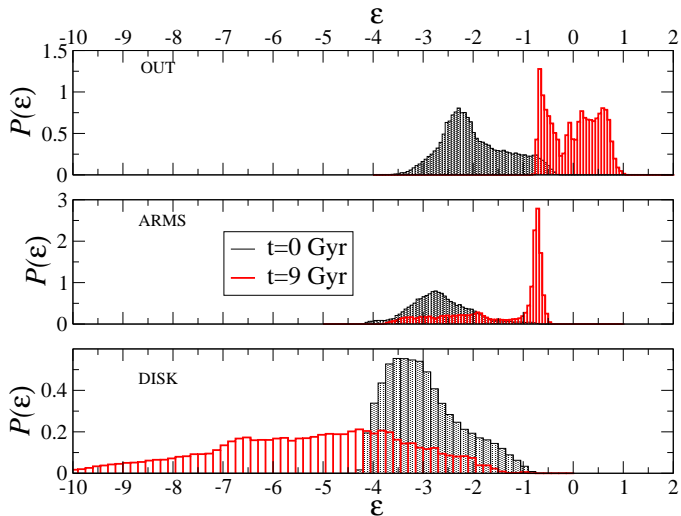


FIG. 18. Particle energy PDF of the GPs in the three different regions at  $t = 0$  and  $t = 9$  Gyr.

gravitational potential [46]. From the Jeans equation (in cylindrical coordinates) we can then derive the circular speed, by neglecting the cross-term  $\langle v_\phi v_R \rangle$  that represents a negligible correction [67], obtaining

$$v_{c,J}^2(R) = \langle v_\phi^2 \rangle - \langle v_R^2 \rangle \left( 1 + \frac{\partial \ln \nu}{\partial \ln R} + \frac{\partial \ln \langle v_R^2 \rangle}{\partial \ln R} \right), \quad (20)$$

where  $\nu = \nu(R, z)$  is the density and we have labeled the circular velocity as  $v_{c,J}$  to recall that it is derived under the assumptions of the Jeans equation.

We have estimated  $v_c$  in Eq.(19) from the direct gravitational force summation and  $v_{c,J}$  in Eq.(20) (by estimating both the radial behavior of the density  $\nu$  and of the radial velocity dispersion  $\langle v_R^2 \rangle$  on the plane (i.e.,  $z \approx 0$ ) and by computing numerically their logarithmic deriva-

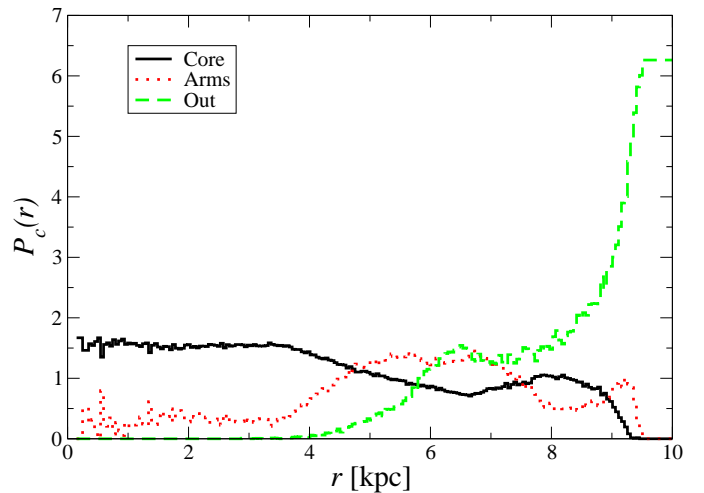


FIG. 19. Conditional probability as a function of the initial distance for a particle to be in the inner, intermediate or outer region of the system at  $t = 9$  Gyr.

tives (for a more detailed discussion see Ref. [68]). Results, as expected, show that  $v_{c,J} \approx v_c$  in the inner disk while at large distances (i.e.,  $r > 30$  kpc)  $v_{c,J} > v_c$ : the deviation of  $v_{c,J}/v_c$  from unity correlates with the amplitude of the mean radial velocity  $\langle v_R \rangle$  that describes the deviation from equilibrium of a system.

## I. Discussion

The main result of our simulations is that a quasistationary rotating disk can be formed from the monolithic collapse of an isolated out-of-equilibrium overdensity of self-gravitating matter with a dissipational gas component. Around such a disk long-lived but nonstationary spiral arms are formed whose velocity field is dominated by rotational motion but that also show large-scale gradients in all velocity components. At larger distances the whole system is surrounded by out-of-equilibrium spiral arms. The physical mechanism that gives rise to such an heterogeneous system is the variation of the system's mean-field potential energy in the short time interval around the global collapse. Such a variation amplifies any initial deviation from spherical symmetry and causes a large change of the particle energy distribution. There are two very different timescales: (1) the characteristic collapse timescale  $\tau \sim 1/\sqrt{G\rho}$  (where  $\rho$  is the initial density); and (2) the life-time of the spiral arms  $t_{arms}$  that we have shown to be  $\gg \tau$ . Because  $\tau \ll t_{arms}$ , the formation of this kind of QSS can be compatible with astrophysical constraints both at small and high redshifts.

As a result of this process the purely nongaseous matter forms a thick disk that is dominated by the (azimuthal) rotational motion but in which there is a large velocity dispersion. Instead, the gas forms a thin disk, almost 2D with a vertical height scale far shorter than

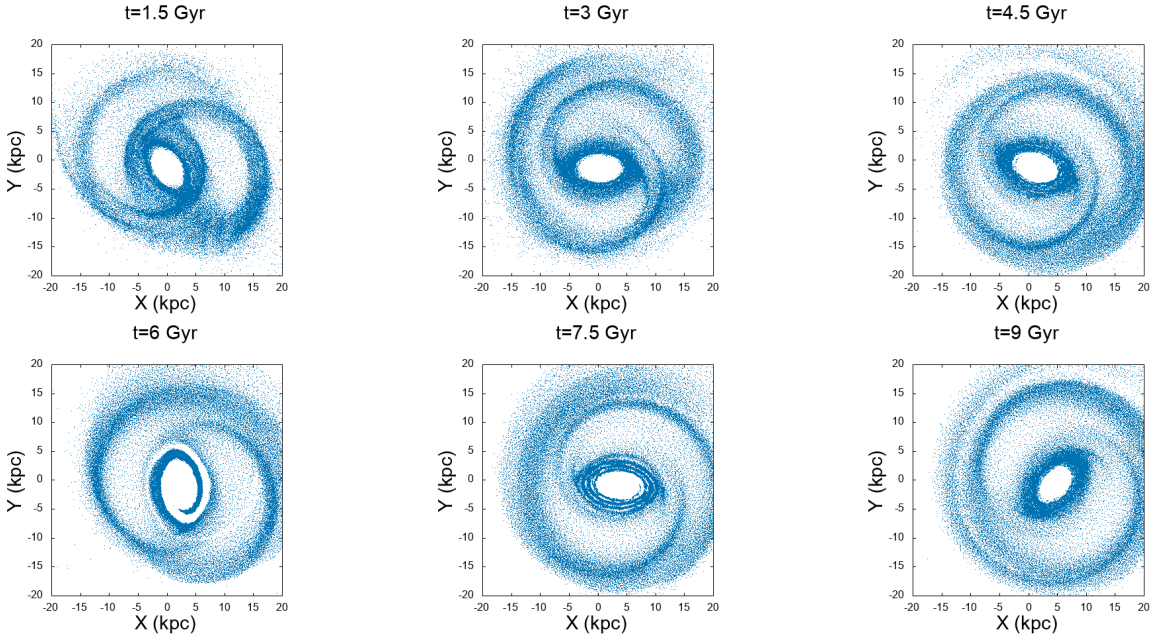


FIG. 20. Evolution of the spiral arms in the  $XY$  plane: the particles belonging to the arms have been identified at  $t = 6$  Gyr and then traced backward or forward in time to  $t = 0$  Gyr and  $t = 9$  Gyr.

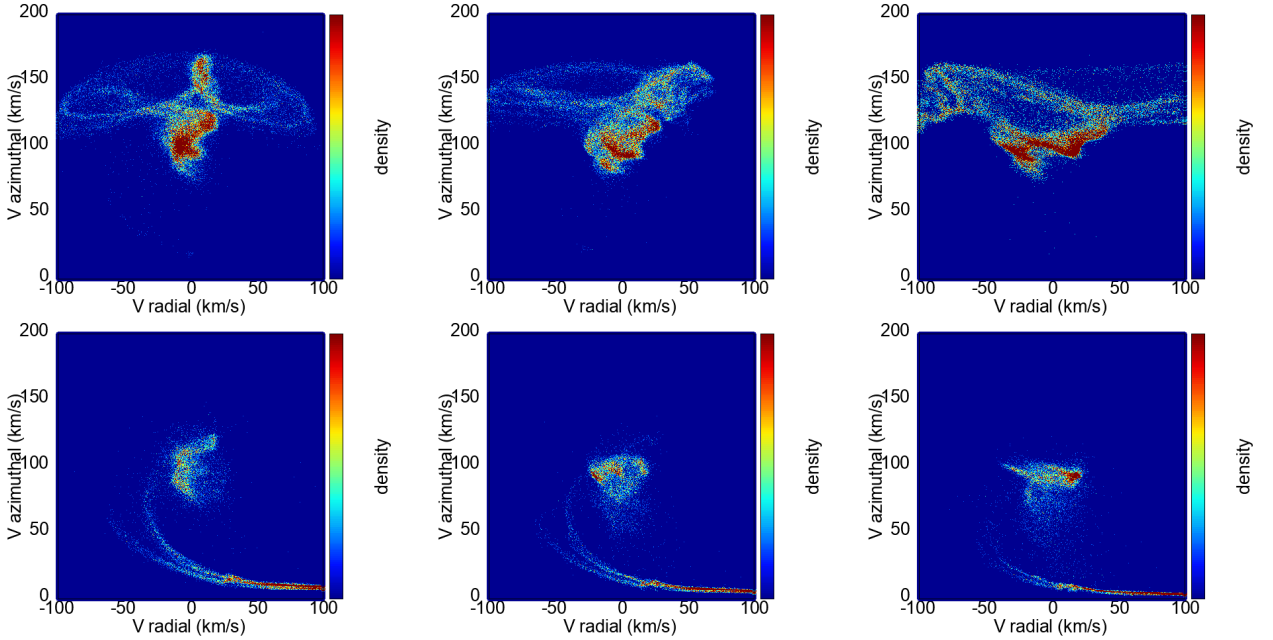


FIG. 21. Projection of the phase-space distribution of the GPs into the  $v_R - v_\phi$  plane. The upper row shows the spiral arms and the bottom row the outer regions and different times: from left to right at  $t = 3, 4.5, 7.5$  Gyr.

the horizontal size, where there are coherent rotational motions and a small velocity dispersion. Such a difference in the density configuration evolution between the nonvolatile matter and the gas occurs because when the system approaches its maximum contraction the latter component increases its density and thus can radiatively cool and sink to the nongaseous clumps. Since the gas is subjected to compression shock and radiative cooling

with consequent kinetic and thermal energy dissipation, it develops a much flatter disk, where rotational motions are coherent and the velocity dispersion is smaller than that of the nongaseous matter. The quasistationary thin gaseous disk is thus embedded in the gravitational field of the thicker nongaseous disk that dominates the system mass and thus the potential energy. The thin disk is in general elliptical, where the eccentricity depends on

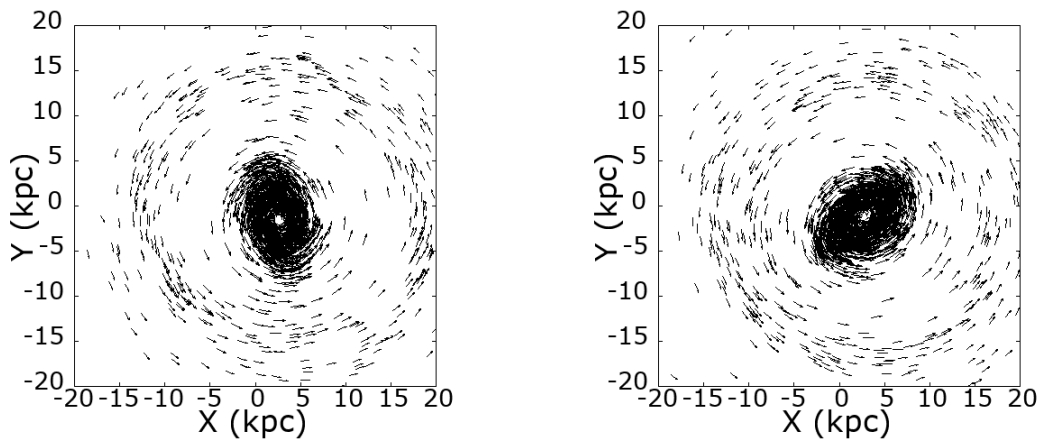


FIG. 22. Projection of two snapshots of the GP component on the  $XY$  plane at  $t = 6, 6.15$  Gyr: the velocity and its direction for a sub-sample of the system's GPs has been shown with an arrow.

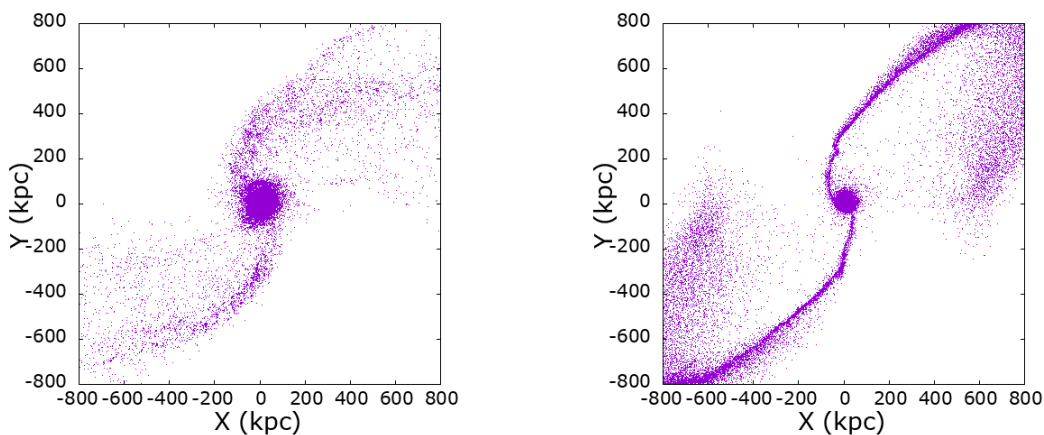


FIG. 23. Projection of the GPs (left panel) and PPs (right panel) on the  $XY$  plane at  $t = 6$  Gyr.

the violence of the collapse, i.e., on how much the system's gravitational radius has contracted, and thus on the shape of the ICs and on the initial angular momentum.

By analyzing the evolution of the spatial distribution of the SPH particles used to represent the gas, we have found that they form long-lived but nonstationary spiral arms. Such structures are formed by particles that have undergone to a similar dynamical history and that, consequently, remain correlated in both position and velocity. Their energy is larger than that possessed by the other particles forming the inner disk, even though they are still bound to the system. They show a rough velocity field in which both radial and rotational motions are time-dependent and correlated. The spiral arms are nonstationary mainly due to this latter characteristic. On the other hand, the long-lived spiral nature of the spiral arms arise from the correlation in phase space that the particles develop during the gravitational collapse. Finally both GPs and PPs form far-out-of-equilibrium spiral arms in the very outermost regions of the system, where the velocity field is dominated by radial motions.

We have discussed in detail the time evolution of a single numerical experiment in which the ICs were constituted by a prolate ellipsoid. We have, however, performed many other simulations and here we summarize our main results.

1. Systems with two-spiral arms, in both the gas and nongaseous components, are formed provided that the starting configuration breaks spherical symmetry in the  $XY$  plane as, for instance, the case of a prolate ellipsoid. Starting with an initial system consisting in an oblate ellipsoid, a multiple-arms system with a ring structure on the  $XY$  plane can be formed, whose velocity field is characterized by a combination of rotational and radial motions. When the initial system presents a configuration more irregular than a simple ellipsoid it evolves acquiring more complex shapes: however, as long as there is a major axis that is enough larger than the others, a two-arms spiral structure is formed. In this regard, we performed some numerical experiments introducing some randomness

in the shape of the ICs by considering uniform but irregular shapes. Results do not change qualitatively but they are quantitatively different: for instance multiple-arm systems may arise and/or the systems can be characterized by subclumps that first collapse independently and then merge (some examples for systems constituted by only PP are reported in Ref. [40]). It should be noticed that in various simulations bars of different size-scale may be formed. If the bar is as large as the system itself, then it presents a transient structure in which radial and rotational motions are of the same order. Instead, in some cases it can be formed a small bar in the inner regions that can typically survive for many dynamical times. A more detailed characterization of these structures will be presented in a forthcoming work.

2. If we give to the ICs some random motions in addition to solid-body rotational velocity, the evolution notably changes only when the kinetic energy associated to the former becomes of the order of the kinetic energy associated to the latter. Figure 24 shows the comparison of the same initial configuration and initial virial ratio, but for one case the kinetic energy is fully rotational and for the other case the kinetic energy is half rotational and half random. One may see that in the former case the phase-space correlation is broken, i.e., the projection of the phase-space distribution in the  $v_R - v_\phi$  plane shows a much less structured shape when the random velocity is larger. Correspondingly the spiral arms are washed out and the gas forms a structure-less disk.
3. If the initial ratio  $Q$  tends to 1 then the system is initially close to a stationary situation. In this condition the self-gravitating particles do not undergo a strong collapse and the gravitational radius of the system remains close to its initial value. Indeed, the system gently changes its phase-space configuration to reach a quasiequilibrium state and its mean field only slightly varies, so that the main source for the large changes of the phase-space properties is not active. In these conditions the system is closer to spherical symmetry but undergoes a small contraction around the rotation axis (see the upper panels of Fig.25): the velocity dispersion of the PP component remains almost isotropic. On the other hand, the GP component, because of energy dissipation, forms a thin disk that is however structureless as the mechanism originating structures like spiral arms is not active, the variation of the system's mean field being too small (see the bottom panels of Fig.25). Figure 26 shows the phase-space distribution projected on the  $v_R - v_\phi$  plane: not surprisingly, this is structureless.
4. If the initial temperature of the gas is too high

so that the internal energy  $u$  becomes of the order of the particles potential energy per unit mass (see Eq.(17)) then the gas diffuses without clustering. On the other hand, when the temperature is lower than  $\sim 10^4$  K the gas behaves almost like the nonvolatile component, since the cooling is not efficient in irradiating away the thermal energy. In this regard, we have performed some simulations with solely self-gravitating gas dynamics (i.e., no gaseous matter). In such a situation, for a typical temperature of the gas of  $T \sim 4 \times 10^4$  K, i.e., such that cooling is very effective, the formation of spiral arms is inhibited and the system becomes isotropic even when the initial density distribution assumes an ellipsoidal shape. These tests show that the non-gaseous matter plays the key role in the determination of the dynamical evolution of the system.

#### IV. CONCLUSIONS

Understanding the origin and evolution of spiral structures has proved to be one of the harder problems in astrophysics. In this work we have studied the formation of long-lived, but nonstationary, spiral arms as a consequence of the rapid and violent collapse of an isolated system. This physical mechanism is different from the slow and soft dynamical evolution that takes place when a bottom-up aggregation process is at work or when a disk at equilibrium is softly perturbed. The key physical mechanism is the rapid variation of the system size during the collapse, corresponding to a large change of the mean-field potential which, in turn, causes a substantial variation of the particle energy distribution and thus of the system phase-space properties.

Typical cosmological scenarios of structure formations, like CDM models, assume that density fluctuations are strongly correlated and give rise to a soft and slow bottom-up clustering mechanism: for this reason the formation of a disk and spiral arms, via a rapid and violent mechanism, investigated in this work has been commonly overlooked in the literature. Halo structures formed in CDM models are almost spherically symmetric and present a quasi-isotropic velocity dispersion, while disks are characterized by close to rotational and very quiet velocity fields. On the other hand, quasistationary disks formed from a fast and violent dynamical mechanism are characterized by having large streaming motions in all velocity components. In standard CDM type models the distribution of gas and nongas matter are completely different, while in the present case they are correlated.

It is interesting to note that the paradigmatic model for nonlinear structure formation in cosmology, i.e., the spherical collapse model (SCM), says that an overdensity that detaches from the cosmological expansions starts behaving like an isolated system when its density contrast is of order unity [16]. This purely gravitational sys-

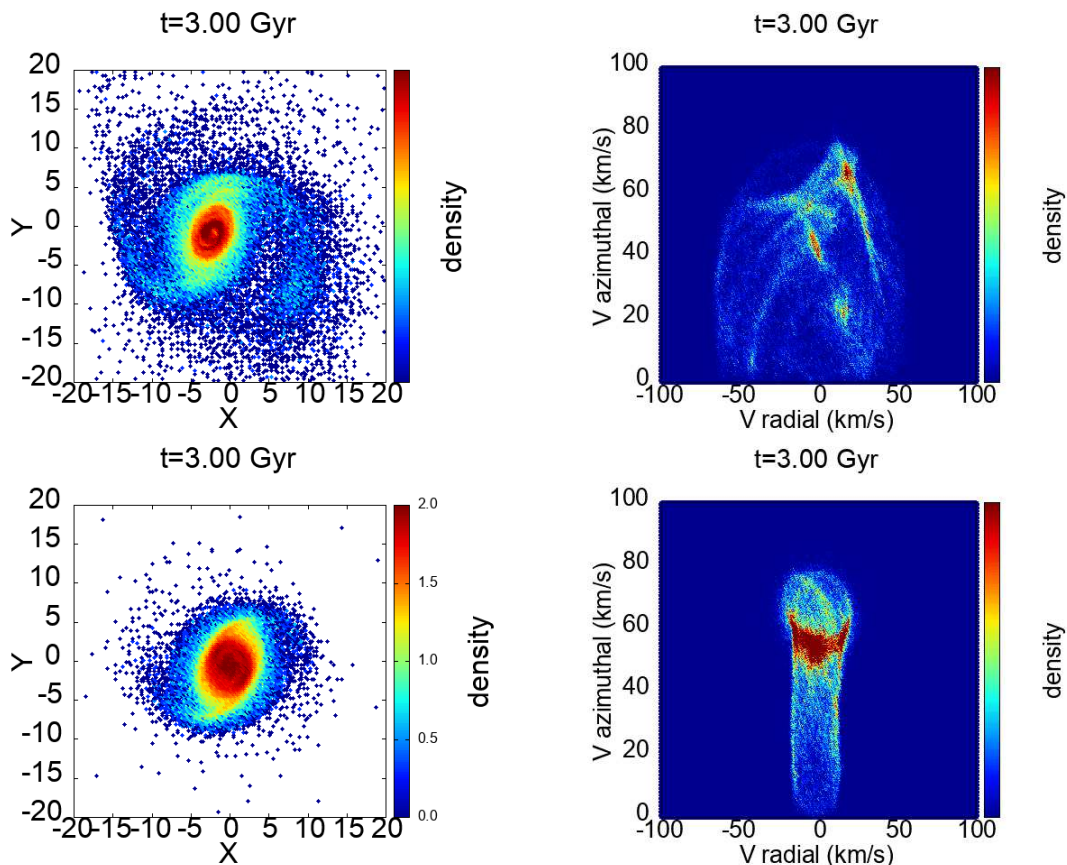


FIG. 24. Comparison of the same initial configuration and initial virial ratio but for one case the kinetic energy is fully rotational (upper panels) and for the other case the kinetic energy is half rotational and half random (bottom panels). In each row, the left panel shows the projection on the  $XY$  plane and the right panel the phase-space distribution projected on the  $v_R - v_\phi$  plane at the same time (i.e.,  $t = 3 \text{ Gyr} \approx 10\tau$ ).

tem thus undergoes a monolithic collapse of the type we have discussed in this work. In CDM scenarios, instead, because density fluctuations are too strongly correlated, clustering proceeds through a bottom-up hierarchical aggregation mechanism. Initial fluctuations must be highly suppressed below some scale as occurs in warm dark-matter-type scenarios, for a SCM-type scenario taking place in a cosmological setting. It is worth noticing that Peebles [69] has recently advocated precisely a monolithic top-down scenario for galaxy formation to overcome the difficulties of standard CDM-like models in explaining the main observations concerning galaxies. In particular, Peebles has proposed a warm dark matter initial mass fluctuations power spectrum that has a sharp cut-off suppressing fluctuations at small enough scales. Such scales are not probed by the cosmic microwave background radiation, and thus do not have to satisfy strong observational constraints, but may be significant for galaxy formation.

Numerical experiments in which the initial conditions represent an isolated overdensity of massive particles with a dissipative gas component represent a suitable playground to explore the combined effects of gravita-

tional and gas dynamics in a system that undergoes to a monolithic collapse. We have identified three essential features for the ICs to form a disk with long-lived spiral arms, otherwise the system forms an ellipsoidal quasistationary configuration without the rich morphological structures observed in the present case.

The first is that they have to be almost uniform, i.e., internal perturbations must be efficiently suppressed. Indeed, density perturbations inside the overdensity grow through gravitational clustering during the collapse, and they form substructures by a hierarchical aggregation process. If the amplitude of the initial density fluctuations is too large and/or their spatial correlations too strong, then they go nonlinear on a scale comparable to the system's size on a time-scale shorter than the collapse time  $\tau$ . At  $t \sim \tau$  the system is made of large sub-clumps, the collapse is halted and the evolution proceeds through an aggregation of the subclumps: in this condition the system mean-field potential is only perturbed but does not undergo a rapid change.

The second condition is that the ICs must break spherical symmetry. Indeed, the variation of the system mean-field potential triggers a large change of the particle en-

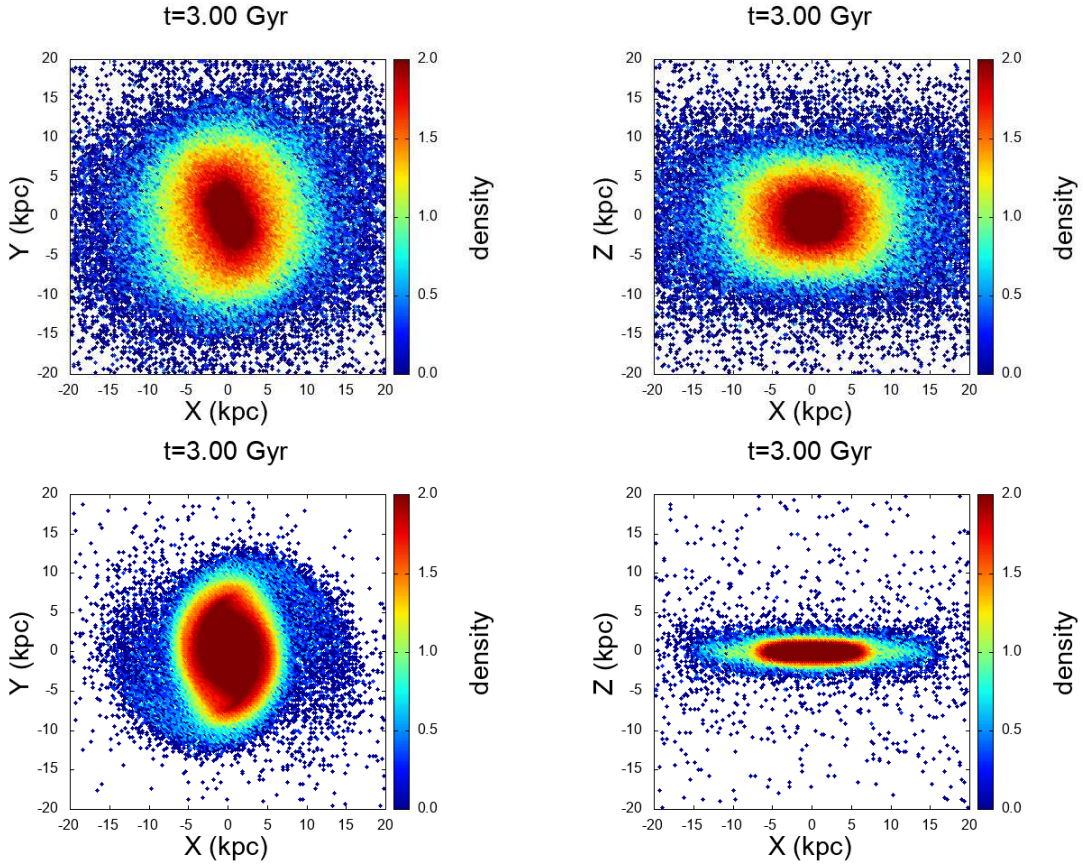


FIG. 25. In this case the initial condition is again an ellipsoid but with a configuration close to quasistationary state, i.e.,  $Q = 1$ . Upper panels: projection of the self-gravitating particles in the  $XY$  plane (left) and  $XZ$  plane (right) at  $t = 3$  Gyr  $\approx 10\tau$ . Bottom panels: same for the gas.

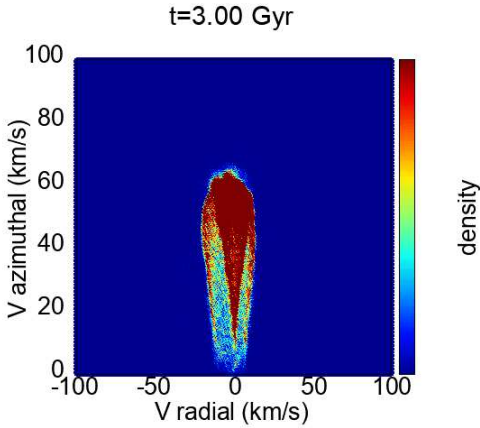


FIG. 26. Phase-space distribution of the gas for the simulation shown in Fig.25 projected on the  $v_R - v_\phi$  plane at  $t = 3$  Gyr  $\approx 10\tau$ .

ergy distribution if a fraction of the particles have a collapse time longer than the bulk of the system mass. In this condition those particles move for a short time interval in a rapidly varying potential field and thus gain

some kinetic energy while all others become more bound. The amount of energy gain depends on the time-lag of a particle to arrive at the center, with respect to the largest fraction of the system mass. For an initially uniform system, such a lag is developed because of the coupling of the system finite size with the growth of internal density fluctuations during the collapse phase. As a result of this complex dynamical mechanism, particles that initially were in the outermost regions arrive later than the others at the center and thus gain the largest amount of energy. For this reason any anisotropy initially characterizing such a particle distribution contributes to the developing of the time lag and it is thus amplified by the collapse dynamics.

Finally, the third condition is that the system has a sufficient initial amount of angular momentum, otherwise rotation is inhibited and a disk cannot form.

Given these three conditions, the dissipationless component of the system gives rise to a thick disk, in which rotational motions are predominant but still with a large velocity dispersion. Such a disk is surrounded by large size out-of-equilibrium spiral arms, with or without bars and/or rings, which are expanding on a secular timescale as the radial motion predominates on the transversal one

[37, 38]. When considering a two-phase system where gas is coupled to the dissipationless component, then the post-collapse configuration shows a more heterogeneous and richer phenomenology. At small distances from the center, gas particles form a quasistationary thin disk in which rotation dominates but where orbits are generically elliptical and thus where radial motions are also present.

Around such a thin disk long-lived but nonstationary spiral arms are formed: they arise from the coherent motions of groups of particles that have undergone a very similar dynamical history. The coherence in the motion of these particles, which maintains the spiral pattern, is originated because they were initially close (in the outer regions of the system) so that they could gain a similar amount of energy during the gravitational collapse remaining correlated in both position and velocity in their subsequent evolution. The life-time of the spiral arms for the system we have considered is much larger than the characteristic collapse timescale  $\tau$  and it is related to the velocity dispersion of the particles in the arms: the larger is the dispersion, the shorter is the life-time. In the numerical experiments we have presented in this work, we have considered the mass and size of a typical spiral galaxy, getting a characteristic collapse timescale of  $\tau \sim 0.5$  Gyr, while the life-time of the spiral arms is  $> 10$  Gyr.

We notice that if the fraction of the system gas is marginal (like is the case of a very high star formation rate leading to a rapid gas to star phase transition), then the nal QSS has the shape of an ellipsoid whose atness parameter, in general, depends on both its initial value and on the amount of initial angular momentum [37]. Thus the monolithic collapse process investigated in this work represents a viable evolutionary path for the formation of elliptical galaxies (or of the almost spherical globular clusters that also have no gas component) as it was firstly argued by [23]. As noticed in [32, 35] the signature of the violent origin of such ellipsoidal QSS is represented by a characteristic  $\sim r^{-4}$  density profile in the external regions and by an almost flat core. Such behaviors are clearly different from the density profile of the halo structures, that are ellipsoidal too, formed through a bottom-up aggregation process in the context of CDM-type cosmological simulations [48]: such a density profile is characterized by a cusp in the inner regions of the type  $\sim r^{-1}$  and by a slower decay in the external regions, i.e  $\sim r^{-3}$ . A further support to a monolithic collapse origin for elliptical galaxies is that in the case of a merger origin of ellipticals from spirals the phase space density, being the merger collisionless, should remain constant, respecting the Boltzmann's collisionless equation, while there are strong hints that in ellipticals it is higher [70]. A more detailed study of the difference between purely gravitational QSS formed through a top-down monolithic collapse and through a bottom-up aggregation mechanism will be presented in a forthcoming work.

Different mechanisms to produce spiral arms and pos-

sibly bars have been proposed in the literature and they all assume that the galactic disk is already formed [47]. A model in which the spiral structure is interpreted as a stationary density wave was introduced by [71] (see [72] for more details): this hypothesizes that the spiral arms arise from a periodic compression and rarefaction of the disk surface density that propagates through the disk and remains stationary over many orbital periods. The spiral arms characterizing the systems that we have discussed are very different from quasi-stationary density waves as they involve the motion of matter and not only of energy. A second mechanism hypothesized to produce spiral arms is given by the effect of local instabilities, or of external perturbations, in a rotating disk. Indeed, self-gravitating disks close to stationary equilibrium and dominated by rotational motions are remarkably responsive to small disturbances so that spiral arms can be transient, recurrent and initiated by swing amplified instabilities in the disk (see, e.g., [43–45, 47] and references therein). In this context, the continuously changing recurrent transient patterns formed in simulations of isolated disk galaxy models, embedded in rigid halos, have a rather quiet velocity field, i.e. there are not present nor large amplitude streaming motions neither a net radial velocity component and the system is dominated by rotational motions. Indeed, the kind of perturbations considered do not sensibly change the system's mean field and give rise to a soft dynamical mechanism that is not able to change the particle energy PDF as it occurs in the violent dynamics we have described in this work. As a result of the violence of the collapse, correlations in phase-space are stronger, and thus the life-time is longer, in the former case than in the latter one. Such correlations correspond to well-defined phase-space structures: in particular, we have highlighted the properties of the phase-space projection into the plane defined by the radial and azimuthal velocity components.

The main difference with the standard CDM scenario is that in that case the disk is embedded in the gravitational potential field of an halo structure, i.e. a system close to spherical with an almost isotropic velocity dispersion. In that situation the gaseous matter forms a disk where rotational motions dominate and whose dynamical properties are determined by the more massive halo structure. On the contrary, in the system we have studied in this paper, the rotating disk is embedded in the gravitational field of a more massive thicker disk that is also rotation dominated in its inner regions. Then, in its outer regions, such a system is not yet relaxed and presents out-of-equilibrium features. Such a situation implies that in those regions it is not possible to simply recover a mass from the measurement of a velocity. This represents an important warning that must be considered in detail when analyzing a given object as in general the assumption of stationary equilibrium with maximal rotational motions is taken for granted in the determination of galaxy masses from observed line-of-sight velocities or velocity dispersion. Indeed, the estimates of

the quantity of dark matter, both in the Milky Way and in external galaxies, are generally based on the assumption that emitters motion is maximally rotational and/or that systems are relaxed into a quasi-stationary equilibrium state. Distance-dependent deviations from these assumptions naturally arise in the systems we have discussed: in such a situation the estimation of the amount of dark matter must be revised taking into account more complex velocity fields and dynamical mechanisms. Of course, from an observational point of view the problem is to detect the presence of nonrotational motions: this is not at all a simple task given the degeneracy between a radial and a rotational velocity field for nonaxisymmetric objects [73].

In this respect, it is worth noticing that the number of revolutions completed by an object orbiting with a velocity of  $\sim 200$  km/s around a galaxy at a distance larger than  $\sim 20$  kpc in a Hubble's time  $\sim 10$  Gyr is of the order of 10 or smaller [40]. If it is not at present possible to theoretically constraint the number of revolutions needed to reach a relaxed configuration from a qualitative point of view, a reasonable requirement is that they must be  $\gg 1$ . This simple observation raises a serious warning about the possibility of considering the outermost regions of a galaxy in a relaxed equilibrium configuration, the hypothesis usually adopted to estimate the amount of dark matter.

There are three main directions that will be pursued in forthcoming works. First, we aim at studying the violent collapse in a full cosmological context, including other astrophysical effects beyond gas dynamics. In this respect, as discussed above, it is necessary to consider density fluctuations with suitable correlations that must be suppressed at small enough scales. Second, we will explore in more details the whole phase-space structure of these

systems, comparing it to both other kind of quasistationary disks originated by different dynamical models (e.g., by the slow and soft dynamics acting in perturbed self-gravitating disks or in disks formed in the framework of CDM models) and to observations of the Milky Way, by considering the forthcoming data provided by the *Gaia* mission [74], and of external galaxies [73]. Such a study is complementary to a wider investigation of different and more complex initial conditions, which include both irregular shapes and nonuniform and correlated matter density fluctuations. Finally we plan a detailed study of external galaxy line-of-sight velocity maps with the aim of developing an alternative way to fit the data than the usually adopted one in which rotational motions are taken to be maximal at all scales.

As a concluding remark it is worth mentioning that the Milky Way velocity field was recently found to exhibit several phase-space structures [75] together with velocity gradients in all three components [68, 76–79]. Such findings can be understood in a model in which the galaxy has a nonstationary nature of the type we discussed in this work, but can also be explained as due to the effect of external perturbers. The forthcoming data of the *Gaia* mission [74] will eventually clarify the situation.

## ACKNOWLEDGMENTS

We thank Volker Springel for making available to us his updated version of the **Gadget-3** code. FSL thanks Lapo Casetti, Edvige Corbelli, Martin López-Corredoira, Michael Joyce, Yuri Baryshev and Zofia Chrobáková for very useful discussions and comments. Finally we thank the anonymous referees of this work who helped us to improve the presentation and discussion of our results.

- 
- [1] T. Padmanabhan, Phys. Rept. **188**, 285 (1990).
- [2] T. Dauxois, S. Ruffo, E. Arimondo, and M. Wilkens, “Dynamics and thermodynamics of systems with long-range interactions: An introduction,” in *Dynamics and Thermodynamics of Systems with Long-Range Interactions* (Springer Berlin Heidelberg, Berlin, Heidelberg, 2002) pp. 1–19.
- [3] A. Campa, A. Giansanti, G. Morigi, and F. Sylos Labini, *Dynamics and Thermodynamics of Systems with Long Range Interactions: Theory and experiments* (AIP Conference Proceedings, 2008).
- [4] A. Campa, T. Dauxois, and S. Ruffo, Phys. Reports **480**, 57 (2009).
- [5] A. Gabrielli, M. Joyce, B. Marcos, and F. Sicard, J. Stat. Phys. **141**, 970 (2010).
- [6] A. Campa, T. Dauxois, D. Fanelli, and S. Ruffo, *Physics of Long-Range Interacting Systems* (Oxford, 2014).
- [7] P. Chavanis, Journal of Statistical Mechanics: Theory and Experiment **5**, R19 (2010).
- [8] B. Marcos, Phys. Rev. E **88**, 032112 (2013).
- [9] Y. Levin, R. Pakter, F. B. Rizzato, T. N. Teles, and F. P. Benetti, Physics Reports **535**, 1 (2014).
- [10] B. Marcos, A. Gabrielli, and M. Joyce, Phys.Rev.E **96**, 032102 (2017).
- [11] P. Di Cintio, S. Gupta, and L. Casetti, MNRAS **475**, 1137 (2018).
- [12] R. A. Capuzzo Dolcetta, *Classical Newtonian Gravity* (Springer International Publishing, 2019).
- [13] D. Lynden-Bell, Mon. Not. R. Astr. Soc. **136**, 101 (1967).
- [14] T. Dauxois, S. Ruffo, E. Arimondo, and M. Wilkens, “Dynamics and Thermodynamics of Systems with Long-Range Interactions: An Introduction,” in *Lecture Notes in Physics*, Vol. 602 (Springer, 2002) pp. 1–19.
- [15] S. Chandrasekhar, Reviews of Modern Physics **15**, 1 (1943).
- [16] P. J. E. Peebles, *The Large-Scale Structure of the Universe* (Princeton University Press, 1980).
- [17] H. L. Wright, B. N. Miller, and W. E. Stein, Astrophys.Space.Sci. **84**, 421 (1982).
- [18] T. Tsuchiya and B. N. Miller, Phys.Rev.Lett. **79**, 3561 (1997).
- [19] T. Tsuchiya and N. Gouda, Phys.Rev.E **61**, 948 (2000).

- [20] M. Joyce and T. Worrakitpoonpon, *Phys.Rev.E* **84**, 011139 (2011).
- [21] T. N. Teles, Y. Levin, and R. Pakter, *Mon.Not.R.Astron.Soc.* **417**, L21 (2011).
- [22] M. Henon, *Ann. Astrophys.* **27**, 1 (1964).
- [23] T. van Albada, *Mon. Not. R. Astr. Soc.* **201**, 939 (1982).
- [24] S. Aarseth, D. Lin, and J. Papaloizou, *Astrophys. J.* **324**, 288 (1988).
- [25] L. Aguilar and D. Merritt, *Astrophys. J.* **354**, 73 (1990).
- [26] C. Theis and R. Spurzem, *Astron. Astrophys.* **341**, 361 (1999).
- [27] C. Boily, E. Athanassoula, and P. Kroupa, *Mon. Not. R. Astr. Soc.* **332**, 971 (2002).
- [28] F. Roy and J. Perez, *Mon. Not. R. Astr. Soc.* **348**, 62 (2004).
- [29] C. M. Boily and E. Athanassoula, *Mon. Not. R. Astr. Soc.* **369**, 608 (2006).
- [30] E. I. Barnes, P. A. Lanzel, and L. L. R. Williams, *Astrophys. J.* **704**, 372 (2009).
- [31] M. Joyce, B. Marcos, and F. Sylos Labini, *Mon. Not. R. Astron. Soc.* **397**, 775 (2009).
- [32] F. Sylos Labini, *Mon. Not. R. Astron. Soc.* **423**, 1610 (2012).
- [33] T. Worrakitpoonpon, *Mon. Not. R. Astr. Soc.* **466**, 1335 (2015).
- [34] D. Merritt and L. A. Aguilar, *Mon. Not. R. Astr. Soc.* **217**, 787 (1985).
- [35] F. Sylos Labini, *Mon. Not. R. Astron. Soc.* **429**, 679 (2013).
- [36] F. Sylos Labini, D. Benhaïem, and M. Joyce, *Mon.Not.R.Astron.Soc.* **449**, 4458 (2015).
- [37] D. Benhaïem and F. Sylos Labini, *Mon.Not.R.Astron.Soc.* **448**, 2634 (2015).
- [38] D. Benhaïem and F. Sylos Labini, *Astron.Astrophys.* **598**, A95 (2017).
- [39] D. Benhaïem, M. Joyce, and F. Sylos Labini, *Astrophys.J.* **851**, 19 (2017).
- [40] D. Benhaïem, F. Sylos Labini, and M. Joyce, *Phys.Rev.E* **99**, 022125 (2019).
- [41] P. Goldreich and D. Lynden-Bell, *Mon.Not.R.Astron.Soc.* **130**, 97 (1965).
- [42] P. Goldreich and D. Lynden-Bell, *Mon.Not.R.Astron.Soc.* **130**, 125 (1965).
- [43] J. A. Sellwood and R. G. Carlberg, *Astrophys.J.* **282**, 61 (1984).
- [44] J. A. Sellwood and R. G. Carlberg, *Astrophys.J.* **785**, 137 (2014).
- [45] J. A. Sellwood and R. G. Carlberg, *Mon.Not.R.Astron.Soc.* **489**, 116 (2019).
- [46] J. Binney and S. Tremaine, *Galactic Dynamics* (Princeton University Press, 2008).
- [47] C. Dobbs and J. Baba, *Pub.Astron.Soc.Austr.* **31**, e035 (2014).
- [48] J. F. Navarro, C. S. Frenk, and S. D. M. White, *Astrophys. J.* **490**, 493 (1997).
- [49] O. J. Eggen, D. Lynden-Bell, and A. R. Sandage, *Astrophys.J.* **136**, 748 (1962).
- [50] N. Katz, *Astrophys.J.* **368**, 325 (1991).
- [51] N. Katz and J. E. Gunn, *Astrophys.J.* **377**, 365 (1991).
- [52] N. Katz, *Astrophys.J.* **391**, 502 (1992).
- [53] V. Springel, *Mon.Not.R.Astron.Soc.* **364**, 1105 (2005).
- [54] N. Katz, D. H. Weinberg, and L. Hernquist, *Astrophys.J.Suppl.* **105**, 19 (1996).
- [55] T. Abel, P. Anninos, Y. Zhang, and M. L. Norman, *New Astronomy* **2**, 181 (1997).
- [56] N. Yoshida, T. Abel, L. Hernquist, and N. Sugiyama, *The Astrophysical Journal* **592**, 645 (2003).
- [57] L. B. Lucy, *Astron.J.* **82**, 1013 (1977).
- [58] R. A. Gingold and J. J. Monaghan, *Mon.Not.R.Astron.Soc.* **181**, 375 (1977).
- [59] J. J. Monaghan, *Ann.Rev.Astron.Astrophys.* **30**, 543 (1992).
- [60] J. J. Monaghan, *Reports on Progress in Physics* **68**, 1703 (2005).
- [61] J. J. Monaghan, *Journal of Computational Physics* **138**, 801 (1997).
- [62] P. J. E. Peebles, *Astrophys.J.* **155**, 393 (1969).
- [63] A. Knebe and C. Power, *Astrophys.J.* **678**, 621 (2008).
- [64] K. M. Kratter, C. D. Matzner, and M. R. Krumholz, *The Astrophysical Journal* **681**, 375 (2008).
- [65] J.-C. Wan, C. Liu, and L.-C. Deng, *Research in Astronomy and Astrophysics* **17**, 079 (2017).
- [66] Y. Levin, R. Pakter, and F. Rizzato, *Phys. Rev.* **E78**, 021130 (2008).
- [67] A.-C. Eilers, D. W. Hogg, H.-W. Rix, and M. K. Ness, *The Astrophysical Journal* **871**, 120 (2019).
- [68] Ž. Chrobáková, M. López-Corredoira, F. S. Labini, H.-F. Wang, and R. Nagy, *Astron.Astrophys* (in the press 2020), arXiv:2007.14825.
- [69] P. J. E. Peebles, “Formation of the large nearby galaxies,” (2020), arXiv:2005.07588.
- [70] R. G. Carlberg, in *Structure and Dynamics of Elliptical Galaxies*, IAU Symposium, Vol. 127, edited by P. T. de Zeeuw (1987) pp. 353–364.
- [71] C. C. Lin and F. H. Shu, *Astrophys.J.* **140**, 646 (1964).
- [72] G. Bertin and C. C. Lin, *Spiral structure in galaxies a density wave theory* (Cambridge, MA MIT Press, 1996).
- [73] F. Sylos Labini, D. Benhaïem, S. Comerón, and M. López-Corredoira, *Astron.Astrophys.* **622**, A58 (2019).
- [74] Gaia Collaboration, T. Prusti, J. H. J. de Bruijne, A. G. A. Brown, A. Vallenari, C. Babusiaux, C. A. L. Bailer-Jones, U. Bastian, M. Biermann, D. W. Evans, and et al., *Astron.Astrophys.* **595**, A1 (2016).
- [75] T. Antoja, A. Helmi, M. Romero-Gómez, D. Katz, C. Babusiaux, R. Drimmel, D. W. Evans, F. Figueras, E. Poggio, C. Reylé, A. C. Robin, G. Seabroke, and C. Soubiran, *Nature* **561**, 360 (2018).
- [76] Gaia Collaboration, D. Katz, T. Antoja, M. Romero-Gómez, R. Drimmel, C. Reylé, G. M. Seabroke, C. Soubiran, C. Babusiaux, P. Di Matteo, and et al., *Astron.Astrophys.* **616**, A11 (2018).
- [77] H.-F. Wang, C. Liu, Y. Xu, J.-C. Wan, and L. Deng, *Monthly Notices of the Royal Astronomical Society* **478**, 3367-3379 (2018).
- [78] M. López-Corredoira and F. Sylos Labini, *Astron.Astrophys.* **621**, A48 (2019).
- [79] M. López-Corredoira, F. Garzón, H. F. Wang, F. Sylos Labini, R. Nagy, Ž. Chrobáková, J. Chang, and B. Villarreal, *Astron.Astrophys.* **634**, A66 (2020).